Biological and Sensory Properties of Bioactive Peptides and Phenolic-Derived Plant Proteins

Lead Guest Editor: Muhammad Al-u'datt
Guest Editors: Inteaz Alli, Sana Gammoh, and Doa'a Al-u'datt

Biological and Sensory Properties of Bioactive Peptides and Phenolic-Derived Plant Proteins

Biological and Sensory Properties of Bioactive Peptides and Phenolic-Derived Plant Proteins

Lead Guest Editor: Muhammad Al-u'datt
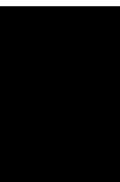Guest Editors: Inteaz Alli, Sana Gammoh, and Doa'a Al-u'datt

María B. Pérez-Gago (iD), Spain
Anand Babu Perumal (iD), China
Gianfranco Picone (iD), Italy
Witoon Prinyawiwatkul, USA
Eduardo Puértolas (iD), Spain
Sneh Punia, USA
Sara Ragucci (iD), Italy
Miguel Rebollo-Hernanz (iD), Spain
Patricia Reboredo-Rodríguez (iD), Spain
Jordi Rovira (iD), Spain
Swarup Roy, India
Narashans Alok Sagar (iD), India
Rameswar Sah, India
El Hassan Sakar (iD), Morocco
Faouzi Sakouhi, Tunisia
Tanmay Sarkar (iD), India
Cristina Anamaria Semeniuc, Romania
Hiba Shaghaleh (iD), China
Akram Sharifi, Iran
Khetan Shevkani, India
Antonio J. Signes-Pastor (iD), USA
Amarat (Amy) Simonne (iD), USA
Anurag Singh, India
Ranjna Sirohi, Republic of Korea
Slim Smaoui (iD), Tunisia
Mattia Spano, Italy
Barbara Speranza (iD), Italy
Milan Stankovic (iD), Serbia
Maria Concetta Strano (iD), Italy
Antoni Szumny (iD), Poland
Beenu Tanwar, India
Hongxun Tao (iD), China
Ayon Tarafdar, India
Ahmed A. Tayel (iD), Egypt
Meriam Tir, Tunisia
Fernanda Vanin (iD), Brazil
Ajar Nath Yadav, India
Sultan Zahiruddin (iD), USA
Dimitrios I. Zeugolis (iD), Ireland
Chu Zhang (iD), China
Teresa Zotta (iD), Italy

Contents

WILEY | Hindawi

Research Article

Improving the Functional and Sensory Properties of Cookies by Ultrasonic Treatment of Whey Proteins

Taha Rababah [ID],[1] Muhammad Al-U'datt [ID],[1] Majdi Al-Mahasneh,[2] Ahmad Alsaad,[3] Sana Gammoh,[1] Hana'a Mahili,[1] Khaled Bny Abdhamead,[4] Ali Almajwal,[5] Tha'er Ajouly,[1] and Vaida Bartkute-Norkuniene[6]

[1]*Department of Nutrition and Food Technology, Jordan University of Science and Technology, P.O. Box 3030, Irbid 22110, Jordan*
[2]*Department of Chemical Engineering, Jordan University of Science and Technology, P.O. Box 3030, Irbid 22110, Jordan*
[3]*Department of Physical Sciences, Jordan University of Science and Technology, P.O. Box 3030, Irbid 22110, Jordan*
[4]*Jadara University, Faculty of Law, P.O. Box 733, Irbid 21110, Jordan*
[5]*College of Applied Medical Sciences, King Saud University, Riyadh, Saudi Arabia*
[6]*Faculty of Business and Technologies, Utena University of Applied Sciences, Utena, Lithuania*

Correspondence should be addressed to Taha Rababah; trababah@just.edu.jo

The profiles of food products are one interesting link that adds a new functional component. Cookies became one of the remarkable foods as a result of their simple preparation, a protracted period, and a sensible acceptance by the population. The effects of sonication on physical and sensory characteristics of cookies to be enhanced were studied. The results showed that cookies prepared with 5 and 10% replacement of sonicated whey protein had significant differences in sensory evaluation especially crumb, but there were no significant differences in the physical characteristics, so we can conclude that sonication will improve sensory properties of cookies. Also, we can conclude that biscuit samples supplemented with 5 or 10% WPC were nutrient-rich. The results of the sensory evaluation showed that the cookie samples supplemented with 5% WPC performed better in most of the characteristics but decreased with an increase in the WPC level. The texture properties of the cookie samples indicated that the control cookies with WPC-supplemented cookies showed no significant differences in most studied properties. It can be concluded that the addition of sonicated whey protein enhanced the physiochemical and sensory properties of cookies.

1. Introduction

Recently, the demand for consuming nutritionally rich products has been increasing among consumers, and these products are ready to eat, have a long shelf life, and are categorized as high and good quality protein contents [1]. Cookies are one of the interesting food products that add a new functional ingredient, because they are easy to prepare, have a long shelf life, and have good acceptance by the population [2], and they are considered as the largest category of snacks around the world [3]. The manufacturing process of cookies was investigated by the authors in [3], and they said that the process was easy and took only 30 min.

First, fat and sugar were being creamed to a smooth consistency, then, eggs and milk were added and mixed, and after that, dry ingredients such as flour, baking powder, and salt were mixed together, followed by adding cream, vanilla extract, and nutmeg and then mixing to form dough. The dough was then placed in greased pans, and eggs were washed; finally, the cookies were baked at 150°C/20 min. In addition, eggs are used instead of water for proper dough formation [1] and milk is added due to its content of protein which contributes to structural properties of products such as emulsion, foaming, and gel properties [4]. Whey is a collective term referring to the serum of watery portion that separates from curd during conventional cheese making [5].

Main proteins present in milk are whey and casein, and also, milk is rich in calcium, phosphorus, essential amino acids, and water-soluble vitamins, which makes whey a highly nutritious product [6]. Whey protein concentrates (WPCs) have been found to be used in biscuits, cookies, cakes, sponges, icings, and glazes to improve texture, flavor, and appearance [7]. Also, whey can be used to produce refreshing beverages [8]. Guimaraes [9] showed that beverages based on whey with at least 51% (m./m.) of content are typically made from ingredients that consist of dairy compounds (liquid or powdered milk and whey). Furthermore, whey is characterized by excellent nutritional and functional properties and low cost of production [10, 11]; however, its nutritional and functional properties can be enhanced by incorporating other ingredients such as fruit pulp and prebiotics [9]. Also, Lagrange [12] showed that in the last decades, the demand for high protein dairy powders increased like a whey protein isolate. Guralnick [13] explained that these powders provide a high-quality protein source and have a wide range of functional properties desired during processing and in finished product applications.

Tirloni [14] explained that whey proteins are also used in sports beverages, due to special functionality and high nutritional values. Wheat flour is considered to be the basic ingredient for bakery products such as chapatis, rotis, paratha, bread, buns, cookies, cakes, patties, and pancakes [15]. The chemical composition of whole-wheat flour is as follows: moisture (9.38–10.43%), ash (1.32–1.85%), crude protein (10.13–14.74%), crude fat (1.96–2.52%), crude fiber (2.31–2.99%), nitrogen-free extract (78.71–85.37%), wet gluten (23.53–38.71%), and dry gluten (7.51–13.52%) among different wheat [16]. On the other hand, ultrasound (US) is defined as waves of a mechanical nature that require an elastic medium to propagate, US waves propagate at frequencies greater than 20 kHz (upper limit of audibility for the human ear), and US has been applied to food technologies due to its mechanical and/or chemical effects on improving the processes of homogenization, mixing, filtration, crystallization, dehydration, and others [17]. Frequency, processing time, and power of ultrasound are factors which have significant effects on food [18]. Ultrasound treatment is one of the nonthermal technologies that are studied regarding microbial inactivation and microstructural changes, so this technology is important in dairy products, which represents one of the most important sectors of the food industry and has a wide range of products developed from various processes [19]. Ultrasound frequency range is divided into two types: low and high frequencies. Low frequencies use intensities below 1 W/cm2 and higher than 100 kHz. High frequencies use intensities higher than 1 W/m2 and between 20 and 500 kHz [20]. Results showed that high pressure and US vibrations significantly affect the physical and structural properties of proteins, When whey protein concentrate was treated with ultrasound, a reduction in molecular size was observed. This indicates that ultrasound increased the particle size and decreased the range for particle size distribution. This resulted in the formation of molecule aggregates [21].

2. Materials and Methods

Soft wheat flour, sugar, and shortening was procured from the local market of Jordan and kept at room temperature for further use. All chemicals used were of analytical grade.

2.1. Sample Preparation of Cookies.
Three levels of whey protein concentrate (WPC) were used to prepare cookies along with wheat flour. Dough was prepared for 30 min and sheeted manually to a thickness of 5 mm by means of a rolling pin. After that, the cookies were cut by using a 50 mm diameter cookie cutter. Then, they were baked at 220°C for 10 min in an oven and cooled at room temperature for one hour and packed in sealed polythene bags for further analysis.

2.2. Proximate Analysis of Cookies.
The approximate composition of samples including moisture content, ash content, crude protein, crude fat, and crude fiber based on the dry weight were measured according to the American Association of Cereal Chemists (2000).

2.3. Spread Factor.
The AACC Method 10-50D (1983) was used to evaluate the cookie width, thickness, and spread factor. The cookie width (W) was measured by placing six cookies edge to edge to get the average width in mm. The cookie thickness (T) was measured by stacking six cookies on top of each other and restacking in different order and remeasuring them to get the average in mm. The spread factor (SF) was determined from width and thickness as shown in the following equation:

$$ SF = \left[\left(\frac{W}{T} \right) \times C.F \times 10 \right]. \tag{1} $$

C.F is the correction factor for adjusting W/T (as is) to constant atmospheric pressure. For this work, C.F was taken to be 1.0.

2.4. Sensory Properties of Cookies

2.4.1. Consumer Test.
The consumer sample population was selected from the database of consumers in Jordan University of Science and Technology, who were 18–60 years of age and of various socioeconomic backgrounds. Consumers responded to an e-mail survey questionnaire including demographics as well as the consumption frequency of biscuits. Only those who consumed biscuits at least once per week were selected to participate in the assessment, with a target of 60 participants (36 males and 24 females).

Consumer testing was conducted at the Jordan University of Science and Technology Sensory Analysis Laboratories. Respondents were provided with ID cards in the order in which they arrive at the test site and directed to

TABLE 1: Definition, evaluation procedure, scale, and references used for the attribute measurement.

Descriptor	Definition	Scales and references	
Appearance whey presence	Visual observation of whey	Absence(0)	Amount as a teaspoon (10)
Mouth texture friability	Ability to generate cheese fragment from the beginning of chewing	Skimmed plain yoghurt Larsa(0)	Curd brand Asturiana (10)
Solubility	Ability of the sample to melt with saliva	Curd Asturiana (5)	
Moistness	Perception of water absorbed or released by that product during early mastication	Banana (0)	Skimmed plain yoghurt Larsa (10)
Graininess	Perception of coarse particles in the mouth	Whey cheese Arquega (5)	
Floury	Perception of floury texture in the mouth	Ripe golden apple (0)	Canned beans without skin (10)
Creaminess	Perception of thickness and smoothness pressing the sample between the tongue and palate	Skimmed plain yoghurt (0)	Spreadable cheese Philadelphia (10)
Taste and aroma			
Acid taste	Basic taste similar to that of diluted aqueous solution of citric acid	0.13 g/L (5)	
Salty taste	Basic taste similar to that of diluted aqueous solution of sodium chloride	0.70 g/L (5)	
Bitter taste	Basic taste similar to that of diluted aqueous solution of caffeine	0.54 g/L (5)	
Fresh cheese flavor	Intensity of the olfactory- gustatory sensation perceived during mastication associated with typical aroma of fresh cheese	Commercial cheese Burgos type (5)	
Milk flavor	Intensity of the olfactory-gustatory sensation perceived during mastication associated with raw milk at room temperature	Absence (0)	Full fat milk (10)
Strange flavor	No typical aromas related to fresh cheese	Absence (0)	Intense (10)
After taste	Intensity of the olfactory-gustatory sensation perceived after mastication and swallowing the sample	Absence (0)	Intense (10)
Persistency	Duration of the olfactory-gustatory sensation perceived after the bolus leaves of the mouth	≤10 s	≥60 s (10)

individual test booths with written instructions and balloting. A blind basis method of analysis was used, where samples were coded with randomly selected 3 digit numbers and balanced ordered testing.

Each consumer was provided with a tray containing 6 pieces of biscuit treatments (for each of sample) in 50 mL plastic sample containers. To eliminate carry over factors, consumers were also provided with unsalted crackers and room temperature water for mouth cleansing between samples. The consumers were asked to record their acceptance and intensity scores for overall impression, overall flavor, overall texture, and overall color (9 point scale with 9 = "like extremely" and 1 = "dislike extremely"); crust and crumb (just about the right scale with 1 = much too rough walls and no pores, 2 = too rough walls and no pores, 3 = just about right, 4 = too soft walls and pores, and 5 = much too soft walls and pores); hardness (just about the right scale with 1 = "much too soft" and 5 = "much too hard"); adhesiveness (just about the right scale with 1 = much too nonadhesive, 2 = too non-adhesive, 3 = just about right, 4 = too adhesive, and 5 = much too adhesive).

2.4.2. Quantitative Descriptive Analysis. The quantitative descriptive analysis was carried out with a panel of trained tasters, which included 15 tasters with previous experience in the sensory evaluation of cookies [22]. The descriptor set was generated according to the standards of sensory analysis. Descriptors and references to an anchor scale are listed in Table 1. The procedures for selection and training of the

judges were in accordance with standard international norms [22]. The trained panel generated the cookie set sensory descriptors, scales, and references to evaluate the sensory profile according to the standard norms [22].

2.5. Statistical Analysis. Data were analyzed using the general linear model (GLM) procedure with the SAS Version 8.2 software package (SAS 2002 Institute Inc., Cary, NC, USA). Means were separated by LSD analysis at a least significant difference of 0.05 *p* value.

3. Results and Discussion

3.1. Effect of WPC on Composition of Cookies. As shown in Table 2 (chemical composition before processing), the moisture content of cookies decreased from 12.50 to 10.55%. Control registered the highest moisture content (12.50%), while the lowest moisture content of 10.55% was found for WPCSH (10%). Our results are in good agreement with the findings of the authors in [23] regarding ash, protein, and fat contents where the proximate composition of samples differed slightly from that of the control sample. Gallagher [24] expressed that an increase in moisture content with the increasing WPC supplementation level may be due to more bound water in the system. Our result is not in good agreement with those of the authors in [25] who expressed that biscuits with WPC are higher in moisture content than those with the control sample. Protein content in cookies increased from 12.71 to 18.57%. The highest value for

Table 2: Chemical composition values before processing.

Sample	Moisture (%)			Ash (%)			Protein (%)			Fat (%)		
Flour (control)	12.50	±	0.90	0.48	±	0.04	12.71	±	1.12	0.91	±	0.08
WPC (5%)	11.80	±	0.76	0.58	±	0.20	15.66	±	1.39	0.98	±	0.09
WPCSL (5%)	11.73	±	0.72	0.61	±	0.17	15.82	±	1.07	0.97	±	0.08
WPCSH (5%)	11.56	±	0.67	0.63	±	0.12	15.71	±	1.11	0.98	±	0.08
WPC (10%)	10.82	±	0.67	0.72	±	0.13	18.48	±	1.14	1.08	±	0.07
WPCSL (10%)	10.62	±	0.71	0.71	±	0.12	18.51	±	1.13	1.10	±	0.07
WPCSH (10%)	10.55	±	0.32	0.69	±	0.24	18.57	±	1.17	1.09	±	0.05

(i) WPC (5%) whey protein concentrate + 95% flour, (ii) WPCSL (5%) with sonication low, (iii) WPCSL (5%) with sonication high, (iv) WPCSL (10%) with sonication low and 10% WPC, and (v) * means ± SD in the same column with the same letters are not significantly different ($P \leq 0.05$).

Table 3: Chemical composition after processing.

Treatment	Moisture (%)				Ash (%)				Protein (%)				Fat (%)			
Flour (control)	4.12	d	±	0.22	1.43	b	±	0.10	15.83	c	±	1.21	1.62	c	±	0.90
WPC (5%)	4.32	c	±	0.23	1.47	ab	±	0.08	18.79	b	±	1.27	1.82	b	±	0.79
WPCSL (5%)	4.49	bc	±	0.22	1.46	ab	±	0.07	18.88	b	±	1.32	1.88	ab	±	1.00
WPCSH (5%)	1.68	B	±	0.24	1.49	ab	±	0.06	18.96	b	±	1.24	1.89	ab	±	1.09
WPC (10%)	4.76	ab	±	0.23	1.52	a	±	0.08	21.74	a	±	1.25	1.96	a	±	0.86
WPCSL (10%)	4.87	a	±	0.27	1.57	a	±	0.08	21.78	a	±	1.29	1.97	a	±	1.04
WPCSH (10%)	4.93	a	±	0.17	1.59	a	±	0.07	21.89	a	±	1.34	1.98	a	±	1.15

(i) WPC (5%) whey protein concentrate + 95% flour, (ii) WPCSL (5%) with sonication low, (iii) WPCSL (5%) with sonication high, (iv) WPCSL (10%) with sonication low and 10% WPC, and (v) *means ± SD in the same column with the same letters are not significantly different ($P \leq 0.05$).

Table 4: Physical characteristics of different levels of replacement.

Treatment	Weight (gm)*			Width (cm)*			Thickness (cm)*			Spread factor*			
Flour (control)	61.82	±	3.11	5.06	±	0.23	0.84	±	0.04	56.11	±	3.51	c
WPC (5%)	62.17	±	3.14	5.31	±	0.22	0.88	±	0.04	56.36	±	3.51	bc
WPCSL (5%)	62.28	±	3.17	5.12	±	0.25	0.87	±	0.03	56.91	±	3.50	bc
WPCSH (5%)	61.23	±	3.22	5.21	±	0.31	0.87	±	0.07	57.26	±	3.15	bc
WPC (10%)	61.21	±	3.25	5.42	±	0.25	0.89	±	0.05	57.81	±	4.02	ab
WPCSL (10%)	60.36	±	3.36	5.22	±	0.31	0.87	±	0.05	58.24	±	4.95	ab
WPCSH (10%)	61.68	±	3.23	5.28	±	0.34	0.90	±	0.07	59.45	±	2.97	a**

(i) WPC (5%) whey protein concentrate + 95% flour, (ii) WPCSL (5%) with sonication low, (iii) WPCSL (5%) with sonication high, (iv) WPCSL (10%) with sonication low and 10% WPC, and (v) *means ± SD in the same column with the same letters are not significantly different ($P \leq 0.05$).

protein content (18.57%) was in WPCSH10%, while the lowest value of 12.71% was in the control sample. The results showed that the protein content of all samples differed greatly. Our results agreed with those of the authors in [7] for WPC-enriched biscuits. Also, fat content of cookies slightly increased from 0.91 to 1.09%. The highest value of fat (1.09%) was observed in WPCSH10%, while the lowest value (0.91%) was observed in control samples. Singh and Mohamed [26] results showed the same variations in fat content of soy-fortified cookies. Finally, ash content of cookies increased from 0.48 to 0.72%. The highest value of ash content (0.72%) was reported in WPC 10%, while the lowest value for ash content (0.48%) was observed in control samples. This result agreed with that of the authors in [25], and they found that ash content in biscuits enriched with the WPC and casein increase.

On the other hand, Table 3 (chemical composition after processing) shows the moisture content of cookies increased from 4.12 to 4.93%, where the highest moisture content (4.93%) was observed in WPCSH10%, while the lowest moisture content of 4.12% was found in control samples. Also, protein content in cookies increased from 15.83 to

21.89%, and this could be linked with increased protein denaturation due to a cavitation effect between myofibrils and thus an increase in protein content [27]. However, the highest value of protein content (21.89%) was observed in WPCSH10%, while the lowest value of (15.83%) was reported in control samples. Moreover, fat content of cookies increased from 1.62 to 1.98%. The highest value of fat (1.98%) was observed in WPCSH10%, while the lowest value (1.62%) was observed in the control sample. The authors in [28] reported that sonication leads to an increase in fat concentration, which was demonstrated by the larger surface area of fat globules after ultrasonication treatment, which resulted in an increase in light scattering. Ash content of cookies increased from 1.43 to 1.59%. The highest value of ash content (1.59%) was reported in WPCSH 10%, while the lowest value of ash content (1.43%) was observed in control samples.

3.2. Effect of WPC on Dimensional Characteristics of Cookies.
Table 4 shows physical characteristics of different levels of replacement, which shows that the thickness of

TABLE 5: Sensory consumer analysis.

Treatment	Overall	Flavor	Texture	Color	Crust (JAR)	Crumb (JAR)	Hardness (JAR)	Color (JAR)	Adhesiveness (JAR)
Flour (control)	6.95 c	6.15 b	6.54 c	6.11 b	2.11 a	1.81 c	3.47 a	2.44 a	3.21 d
WPC (5%)	7.11 bc	6.18 b	6.62 bc	6.14 ab	2.13 a	1.88 bc	3.35 a	2.41 a	3.38 c
WPCSL (5%)	7.17 bc	6.20 b	6.68 ab	6.17 ab	2.17 a	1.94 b	3.31 ab	2.38 a	3.41 bc
PCSH (5%)	7.26 b	6.21 b	6.69 ab	6.15 ab	2.18 a	1.99 b	3.27 b	2.37 a	3.48 b
WPC (10%)	7.32 ab	6.37 a	6.72 ab	6.25 a	2.13 a	2.06 ab	3.22 bc	2.31 ab	3.53 b
WPCSL (10%)	7.38 a	6.35 a	6.81 a	6.27 a	2.14 a	2.13 a	3.21 bc	2.31 ab	3.64 a
WPCSH (10%)	7.45 a	6.36 a	6.85 a	6.31 a	2.15 a	2.18 a	3.13 c	2.25 b	3.68 a

(i) WPC (5%) whey protein concentrate + 95% flour, (ii) WPCSL (5%) with sonication low, (iii)WPCSL (5%) with sonication high, (iv) WPCSL (10%) with sonication low and 10% WPC, and (v) * means in the same column with the same letters are not significantly different ($P \leq 0.05$).

cookies increases with an increase in the WPC supplementation level in wheat flour. However, the findings of the authors in [25] agreed with our results. Significant difference in thickness was observed for samples WPC, WPCSL, and WPCSH, and the obtained results are similar to those found by the authors in [29]who stated that the thickness of WPC-fortified biscuits was greater than that of control biscuits. As biscuits shrunk (diameter decreasing), the decrease in diameter was compensated by the expansion of the thickness, which was the cause of the increased thickness. On the other hand, each decrease in weight of cookies showed an increase in the level of WPC supplementation, and there were significant differences in weight in WPC, WPCSL, and WPCSH, which can be related to the addition of excess water in the formulation of WPC-fortified dough than control biscuit dough [29]. Mishra and Chandra [30] reported that there was a decrease in the diameter in rice bran and soy-fortified biscuits. There was an increase in the spread factor in WPC-supplemented cookies, and a significant difference in weight was observed for samples WPC, WPCSL, and WPCSH and width of cookies with an increase in the level of WPC supplementation. A significant difference in width was also observed for samples WPC, WPCSL, and WPCSH. There is a significant difference in the spread ratio for all cookies, and our results are in compliance with those of the authors in [31] who reported that there was a significant increase observed ($P \leq 0.05$) as the levels of whey protein concentrates increased. Maybe the increase in the rate of prevalence in the definition files is complementary because of the link for WPC significant reduction in the thickness of the complementary profile link for WPC. Similar results were observed in the rate of prevalence by the authors in [32] in the definition of complementary file link powder islands. Also, the author in [33] noticed an increase in the value of the factor in the spread of complementary millet flour biscuits.

3.3. Effect of WPC Sensory Perception of Cookies. The study of consumers' perception can be of major worth to industrial community since it helps in identifying the negative and positive factors that guide the consumer behavior and purchase habits [34]. The results for the sensory evaluation of cookies are given in Table 5 (sensory consumer analysis), and the overall mean score increased from 6.95 to 7.45. The highest score (7.45) was observed in WPCSH 10%, while the lowest mean score (6.95) was observed in control, and flavor increased from 6.15 to 6.37. The highest score (6.37) was observed in WPC 10%, while the lowest mean score (6.15) was observed in control. The mean score of texture increased from 6.54 to 6.85 with the increasing level of WPC supplementation. The highest score of 6.85 was noticed in WPCSH10%, while the lowest mean score (6.54) was noticed in control. The mean score of color increased from 6.11 to 6.31. The highest score (6.31) was observed in WPCSH 10%, while the lowest mean score

(6.11) was observed in control. The crust (JAR) mean score increased from 2.11 to 2.18. The highest score (2.18) was observed in WPCSH 5%, while the lowest mean score (2.11) was observed in control. The crumb (JAR) mean score increased from 1.81 to 2.18. The highest score (2.18) was observed in WPCSH 10%, while the lowest mean score (1.81) was observed in control. The mean score of hardness decreased from 3.47 to 3.12 with the increasing level of WPC supplementation. The lowest score of 3.12 was noticed in WPCSH10%, while the highest mean score (3.47) was noticed in control. The color (JAR) mean score decreased from 2.44 to 2.25. The lowest score (2.25) was observed in WPCSH 10%, while the highest mean score (2.44) was observed in control, and the adhesiveness mean score increased from 3.21 to 3.68. The highest score (3.68) was observed in WPCSH 10%, while the lowest mean score (3.21) was observed in control. The findings obtained from the current work agree well with those of Singh et al. [35]who found the overall acceptability score of sensory evaluation in soy flour-fortified biscuits. Ahmed and Ashraf [31] found that the significant difference in sensory evaluation between samples (5% and 10%) and results regarding color could be related to the Maillard reaction between reducing sugars and proteins.

4. Conclusion

From the present study, it can be concluded that 5% WPC-supplemented cookie samples are nutritionally rich. Sensory evaluation results revealed that 5% WPC-supplemented cookie samples scored highest in most of the attributes. Diameter, thickness, and weight of the cookie samples decreased with an increase in the WPC level. The textural characteristics of cookie samples indicated that control and WPC-supplemented cookies did not show significant differences. This study concluded that the supplementation level of 5% WPC results in acceptable sensory, textural, and physiochemical characteristics.

Data Availability

The data are available upon request from the corresponding author.

Conflicts of Interest

The authors declare that they have no conflicts of interest.

Acknowledgments

References

[1] N. Chopra, B. Dhillon, R. Rani, and A. Singh, "Physico-nutritional and sensory properties of cookies formulated with quinoa, sweet potato and wheat flour blends," *Current Research in Nutrition and Food Science Journal*, vol. 6, no. 3, pp. 798–806, 2018.

[2] M. M. C. de Almeida, C. R. L. Francisco, A. de Oliveira et al., "Textural, color, hygroscopic, lipid oxidation, and sensory properties of cookies containing free and microencapsulated chia oil," *Food and Bioprocess Technology*, vol. 11, no. 5, pp. 926–939, 2018.

[3] B. D. Igbabul, B. M. Iorliam, and E. N. Umana, "Physicochemical and sensory properties of cookies produced from composite flours of wheat, cocoyam and african yam beans," *Journal of Food Research*, vol. 4, no. 2, p. 150, 2015.

[4] A. Gani, A. A. Broadway, M. Ahmad et al., "Effect of whey and casein protein hydrolysates on rheological, textural and sensory properties of cookies," *Journal of Food Science & Technology*, vol. 52, no. 9, pp. 5718–5726, 2015.

[5] K. Chauhan and E. Chawla, "Acceptability appraisal and nutritional quality of food products incorporated with whey protein concentrate and soy flour," *Journal of Food Science Research*, vol. 2, pp. 164–168, 2011.

[6] L. Davis, "Fortifying grain-based with whey protein," *AACC*, vol. 49, pp. 55–58, 2004.

[7] B. Munaza, S. G. M. Prasad, and B. Gayas, "Whey protein concentrate enriched cookies," *International Journal of Scientific and Research Publications*, vol. 2, pp. 165–173, 2012.

[8] I. Jeličić, R. Božanić, M. Brnčić, and B. Tripalo, "Influence and comparison of thermal, ultrasonic and thermo-sonic treatments on microbiological quality and sensory properties of rennet cheese whey," *Mljekarstvo: Časopis Za Unaprjeđenje Proizvodnje I Prerade Mlijeka*, vol. 62, no. 3, pp. 165–178, 2012.

[9] J. T. Guimarães, E. K. Silva, C. S. Ranadheera et al., "Effect of high-intensity ultrasound on the nutritional profile and volatile compounds of a prebiotic soursop whey beverage," *Ultrasonics Sonochemistry*, vol. 55, pp. 157–164, 2019.

[10] J. S. S. Yadav, S. Yan, S. Pilli, L. Kumar, R. D. Tyagi, and R. Y. Surampalli, "Cheese whey: a potential resource to transform into bioprotein, functional/nutritional proteins and bioactive peptides," *Biotechnology Advances*, vol. 33, no. 6, pp. 756–774, 2015.

[11] A. Brandelli, D. J. Daroit, and A. P. F. Corrêa, "Whey as a source of peptides with remarkable biological activities," *Food Research International*, vol. 73, pp. 149–161, 2015.

[12] V. Lagrange, D. Whitsett, and C. Burris, "Global market for dairy proteins," *Journal of Food Science*, vol. 80, no. S1, pp. A16–A22, 2015.

[13] J. R. Guralnick, R. R. Panthi, F. Bot et al., "Pilot-scale production and physicochemical characterisation of spray-dried nanoparticulated whey protein powders," *International Journal of Dairy Technology*, vol. 74, no. 3, pp. 581–591, 2021.

[14] E. Tirloni, M. Vasconi, P. Cattaneo et al., "A possible solution to minimise scotta as a food waste: a sports beverage," *International Journal of Dairy Technology*, vol. 73, no. 2, pp. 421–428, 2020.

[15] J. A. Awan, U. A. Rehman, U. S. Rehman, M. I. Siddique, and A. S. Hashmi, "Evaluation of biscuits prepared from composite flour containing moth bean flour," *Pakistani Journal of Agriculture Science*, vol. 32, Article ID 199, 1995.

[16] K. Kamaljit, S. BaljeetBaljeet, and K. AmarjeetAmarjeet, "Preparation of bakery products by incorporating pea flour as a functional ingredient," *American Journal of Food Technology*, vol. 5, no. 2, pp. 130–135, 2010.

[17] M. Gallo, L. Ferrara, and D. Naviglio, "Application of ultrasound in food science and technology: a perspective," *Foods*, vol. 7, no. 10, pp. 164–182, 2018.

[18] L. M. Carrillo-Lopez, I. A. Garcia-Galicia, J. M. Tirado-Gallegos et al., "Recent advances in the application of ultrasound in dairy products: effect on functional, physical, chemical, microbiological and sensory properties," *Ultrasonics Sonochemistry*, vol. 2021, Article ID 105467, 2021.

[19] J. T. Guimarães, H. Scudino, G. L. Ramos et al., "Current applications of high-intensity ultrasound with microbial inactivation or stimulation purposes in dairy products," *Current Opinion in Food Science*, vol. 42, pp. 140–147, 2021.

[20] T. S. Awad, H. A. Moharram, O. E. Shaltout, D. Asker, and M. M. Youssef, "Applications of ultrasound in analysis, processing and quality control of food: a review," *Food Research International*, vol. 48, no. 2, pp. 410–427, 2012.

[21] A. R. JambrakJambrak, T. J. Mason, V. Lelas, L. Paniwnyk, and Z. Herceg, "Effect of ultrasound treatment on particle size and molecular weight of whey proteins," *Journal of Food Engineering*, vol. 121, no. 1, pp. 15–23, 2014.

[22] C. M. O'Brien, D. Chapman, D. P. Neville, M. K. Keogh, and E. K. Arendt, "Effect of varying the microencapsulation process on the functionality of hydrogenated vegetable fat in shortdough biscuits," *Food Research International*, vol. 36, no. 3, pp. 215–221, 2003.

[23] R. S. Shikha and M. P. S. Yadav, "Effects of whey supplementation on physico-chemical evaluation of developed cookies," *International Journal of Home Science*, vol. 4, no. 2, pp. 130–132, 2018.

[24] E. Gallagher, S. Kenny, and E. K. Arendt, "Impact of dairy protein powders on biscuit quality," *European Food Research and Technology*, vol. 221, no. 3-4, pp. 237–243, 2005.

[25] S. Mahmood, M. Sadiq ButtSadiq Butt, F. Muhammad Amuhammad A, and H. Nawaz, "Baking and storage stability of retinyl acetate (vitamin A) fortified cookies," *Pakistan Journal of Nutrition*, vol. 7, no. 4, pp. 586–589, 2008.

[26] M. Singh and A. Mohamed, "Influence of gluten-soy protein blends on the quality of reduced carbohydrates cookies," *LWT - Food Science and Technology*, vol. 40, no. 2, pp. 353–360, 2007.

[27] A. Filomena-Ambrosio, L. Diaz, C. A. Puig Gómez, and I. Sotelo-Díaz, "Efecto de ultrasonido sobre la actividad ATP-asa y propiedades funcionales en surimi de tilapia (*Oreochromis niloticus*)," *Revista Vitae*, vol. 19, no. 1, pp. S379–S381, 2012.

[28] M. Cameron, L. D. McMaster, and T. J. Britz, "Impact of ultrasound on dairy spoilage microbes and milk components," *Dairy Science & Technology*, vol. 89, no. 1, pp. 83–98, 2009.

[29] V. R. Parate, D. K. Kawadkar, and S. S. Sonawane, "Study of whey protein concentrate fortification in cookies variety biscuits," *International Journal of Food Engineering*, vol. 7, no. 2, 2011.

[30] N. Mishra and R. Chandra, "Development of functional cookie from soy flour & rice bran," *International Journal of Agriculture and Food Science*, vol. 2, pp. 14–20, 2012.

[31] H. A. M. Ahmed, S. A. Ashraf, and A. I. AwadelkareemAlamMustafa, "Physico-chemical, textural and sensory characteristics of wheat flour biscuits supplemented with different levels of whey protein concentrate," *Current Research in Nutrition and Food Science Journal*, vol. 7, no. 3, pp. 761–771, 2019.

[32] S. Kumari and R. B. Grewal, "Nutritional evaluation and utilization of carrot pomace powder for preparation of high fiber cookies," *International Journal of Food Science and Technology*, vol. 44, pp. 56–58, 2007.

[33] A. P. Alobo, "Effect of sesame seed flour on millet biscuit characteristics," *Plant Foods for Human Nutrition*, vol. 56, no. 2, pp. 195–202, 2001.

[34] Y. J. D. Sales, F. J. B. Corrêa, E. R. Tavares-Filho et al., "Insights of Brazilian consumers' behavior for different coffee presentations: an exploratory study comparing hard laddering and completion task," *Journal of Sensory Studies*, vol. 35, no. 6, Article ID e12611, 2020.

[35] B. Singh, M. Bajaj, A. Kaur, S. Sharma, and J. S. Sidhu, "Studies on the development of high-protein biscuits from composite flours," *Plant Foods for Human Nutrition*, vol. 43, no. 2, pp. 181–189, 1993.

WILEY | Hindawi

Research Article

Evaluation of Natural Peptides to Prevent and Reduce the Novel SARS-CoV-2 Infection

María Paredes-Ramos ⬛,[1,2] **Enma Conde Piñeiro** ⬛,[3] **Horacio Pérez-Sánchez** ⬛,[4] **and José M. López-Vilariño** ⬛[2]

[1]*METMED Research Group, Physical Chemistry Department, Universidade da Coruña (UDC), Campus da Zapateira, A Coruña, Spain*
[2]*Hijos de Rivera S.A.U., C/José María Rivera Corral 6, A Coruña, Spain*
[3]*GLECEX (Global and Ecofriendly Natural Extracts S.L.), Edificio CITI, Parque Tecnolóxico de Galicia, San Cibrao das Viñas, Ourense, Spain*
[4]*Structural Bioinformatics and High-Performance Computing Research Group (BIO-HPC), Computer Engineering Department, Universidad Católica San Antonio de Murcia (UCAM), Campus de los Jerónimos s/n, Murcia, Spain*

Correspondence should be addressed to María Paredes-Ramos; mparedes@estrellagalicia.es

In a preventive context, natural peptides can play a major role against SARS-CoV-2, so their character of GRAS (generally recognized as safe) means they would not need innocuity analyses to be employed. This study analyses the potential of pea peptides, LSDRFS and SDRFSY, and amaranth peptides, GGV, IGV, IVG, VGVL, and VIKP, against the SARS-CoV-2 hosts, ACE2 (angiotensin-converting enzyme 2), ACE (angiotensin-converting enzyme), and CD26 (cluster of differentiation 26), and SARS-CoV-2 enzymes, spike glycoprotein and 3CLpro (3-chymotrypsin-like protease). Also, currently used drugs were analysed to contrast drug and peptide behaviour. Employing docking, virtual screening, and molecular dynamics assays, SDRFSY, LSDRFS, and VIKP were detected as potential bioactive peptides by blocking ACE2 and CD26 or reducing the inflammation associated with COVID-19. Enzyme inhibition analyses were also performed, proving the ability of SDRFSY and LSDRFS as ACE2-blocking agents against the spike glycoprotein with inhibition capacities above 80%.

1. Introduction

The high transmission (R0 1.5–6.8) [1, 2] and mortality rates (1–3%) [3] of SARS-CoV-2 had caused a global epidemic. Although several vaccines were developed in a record time, they are not yet available in many parts of the world, so another strategy is required not only to treat COVID-19 patients, but also to prevent the infection of healthy individuals and the reinfection of recovered patients or, at least, to mitigate the harmful effects of the infection.

Great efforts were done by the scientific community to reposition several approved antiviral and anti-inflammatory drugs [4–7]. In this regard, it is well known that some hydrolysed peptides show very high bioactivity when interacting with different human proteins, generating functional benefits in some cases and food allergies in others [8]. Therefore, these peptides could be a good option to take a step forward against SARS-CoV-2 infection. They are directly extracted from natural sources, with no modification of their molecules, so they are not structurally optimized to exert a certain effect and they possess less efficacy than drugs. Nevertheless, the absence of toxic effects related to their consumption makes them excellent candidates to be used as a preventive treatment or even as a treatment for those patients with minor symptoms, acting similarly as cough syrups for mild colds.

To fight this novel coronavirus, two different strategies can be applied: the direct treatment of the virus or the

treatment of the host. Several studies were performed to identify the main receptors of both, and among them, spike glycoprotein, 3-chymotrypsin-like protease (3CLpro), RNA-dependent RNA polymerase (RdRp), and papain-like protease (PLpro) are signalled as the key proteins of the virus. The spike glycoprotein is located on the outer envelope of the virion and contributes to the cell receptor binding, and the 3CLpro enzyme is indispensable to the viral replication and infection process, thereby making them ideal targets for antiviral therapy [9]. Among the host receptors, angiotensin-converting enzyme 2 (ACE2) and dipeptidyl peptidase, known as cluster of differentiation 26 (CD26), are identified as the most important human cell proteins employed as hosts by SARS-CoV-2 [5, 10–13].

Also, critical patients of COVID-19 show extremely high inflammatory parameters, including creatine-reactive protein (CRP) and proinflammatory cytokines (e.g., IL-6 and IL-8) [14, 15]. These proinflammatory cytokines are triggered by the nuclear factor kappa B (NF-kB), and thus, NF-kB can be also an appropriate target to overcome not the SARS-CoV-2 itself but one of their acutest side effects [16]. One of the cell enzymes that mediate the NF-kB pathway is angiotensin-converting enzyme (ACE), so its inhibition would reduce the production of the proinflammatory cytokines already mentioned [17–20]. Hence, ACE is also considered a promising host target.

To find inhibitors for these receptors, computer-aided methods are required. Since the 1990s, huge efforts have been made to test an almost unlimited number of drug-like compounds in an automatic way [21]. Hence, computer-aided drug design (CADD) software is nowadays commonly employed for discovering the bioactive molecules, which can then be employed for the pharmaceutical industry as drugs or for the food industry as nutraceutical supplements or functional food/beverages.

Accordingly, a computational approach rooted in molecular docking-based virtual screening is employed to examine the receptors, namely, 3CLpro (PDB code: 6lu7), ACE2 (PDB code: 6m18), spike glycoprotein (PDB code: 6vsb), CD26 (PDB code: 6l8q), and ACE (PDB code: 1o8a). As inhibitors, a library of pea and amaranth peptides was studied, including LSDRFS, SDRFSY, GGV, IGV, IVG, VIKP, and VGVL. Their computed binding affinities and docking poses were compared to FDA-approved drugs. Then, in vitro assays were performed to test the capacity of these peptides to inhibit the spike glycoprotein-ACE2 interaction.

2. Materials and Methods

2.1. Resources and Programs.
UniProt Knowledgebase (UniProtKB), Swiss Protein (SwissProt) database, ChemSpider database, and Research Collaboratory for Structural Bioinformatics Protein Data Bank (RCSB PDB) were searched.

Openbabel GUI 2.4.1 [22], Acpype [23], Gromacs 2018 [24–26], Chimera UCSF 1.13.1 [27], AutoDock Tools 4.2 [28], AutoDock Vina 2.0 [29], PyMOL 2.3 (The PyMOL Molecular Graphics System, version 2.3 Schrödinger, LLC), Python 2.7.6

(Python Software Foundation), PoseView 1.1.2 (ZBH University of Hamburg, BioSolveIT GmbH), Omega 2.5.1.4 (OpenEye Scientific Software) [30], PLIP 1.3.2 [31], Maestro suite 2019.4, Schrödinger LLC, and the Shuttlemol suite of HPC scripts for virtual screening (https://bio-hpc.eu) were used.

2.2. Materials and Reagents.
Synthetic GGV, VIKP, LSDFRS, and SDFRSY peptides were purchased from APeptide Co. Ltd. (Shanghai, China) and presented a purity degree above 95%. The Spike glycoprotein-ACE2 binding assay kit was purchased from RayBiotech® (Atlanta, United States) and the ACE2 inhibitor screening kit from AssayGenie Ltd. (London, United Kingdom).

2.3. Molecular Modelling

2.3.1. Selection of Ligands.
Several amaranth and pea peptides were identified as bioactive peptides in numerous studies. Some amaranth peptides are well known for their 3-hydroxy-3-methylglutaryl reductase (HMGCR) and angiotensin-converting enzyme (ACE) inhibition capacities, thus reducing cholesterol production and hypertension [32–37]. Several pea peptides are proved to be ACE inhibitors but also ACE2 enhancers, boosting Ang 1–7 and Ang 1–9 production and consequently acting as vasodilators [38, 39].

Accordingly, GGV, IGV, IVG, VIKP, and VGVL from amaranth and LSDFRS and SDFRSY from pea are selected as ligands.

2.3.2. Selection of Receptors.
There are two different target groups that can be employed to overcome the COVID-19 infection: (1) receptors of the virus and (2) receptors of the host [5, 10–13].

The spike glycoprotein (protein S) is mainly responsible for the SARS-CoV-2 entry at the host receptor, so it fuses the virus and the host membranes [40, 41]. Accordingly, this receptor is selected for docking studies (PDB code: 6vsb). Also, there are several virus proteins (3CLpro, RdRd, and PLpro) that are considered important factors for the infection [5, 42]. Among them, the 3CLpro is considered the key for virus replication, so it is selected as a virus receptor for docking analysis (PDB code: 6lu7).

As host enzymes, angiotensin-converting enzyme 2 (ACE2) [40, 43], dipeptidyl peptidase (CD26) [13, 44, 45], and angiotensin-converting enzyme (ACE) [19] are identified as the most important human cell enzymes, so PDB codes 6m18, 6l8q, and 1o8a corresponding to these receptors were downloaded from RCSB.

2.3.3. Molecular File Preparation.
3CLpro (PDB code: 6lu7), ACE2 (PDB code: 6m18), spike glycoprotein (PDB code: 6vsb), CD26 (PDB code: 6l8q), and ACE (PDB code: 1o8a) were downloaded from RCSB.

Ligands were removed from pdb files employing PyMOL 2.3. Then, AutoDock Tools 4.2 was used to remove water molecules, add hydrogens, assign AD4 type to all atoms,

compute Gasteiger charges, and save protein files both in pdb and pdbqt formats.

Ligand molecules were downloaded from ChemSpider in mol format and converted to sdf format using the Openbabel GUI 2.4.1. Then they were converted to mol2 format with the Molconvert script from ChemAxon and minimized in the Merck Molecular Force Field (mmff94). AutoDock Tools 4.2 was employed to convert files to pdbqt format.

2.3.4. Blind Docking Analysis.
A blind docking (BD) study was performed to detect the regions of interaction between ligands and the aforementioned receptors: ACE, ACE2, spike glycoprotein, CD16, and 3CLpro [46].

Series of single docking simulations were performed in each alpha carbon of the protein, detecting the most favourable binding pockets in terms of bond energy but also the spatial conformation of the ligand and its bound residues. Affinities of ligand-protein interactions are determined with AutoDock 4.2 and individual energies of each bonded residue are calculated with PoseView 1.1.2, representing global bond energy and key residues bond energy, respectively.

2.3.5. Virtual Screening Analysis.
To delve deeper into the binding pockets of each ligand, virtual screening (VS) studies were performed, allowing ligands to rotate and move within a box of 30 Å side and increasing the exhaustiveness of the blind docking analysis. The coordinates employed in this step had been obtained from the previous blind docking analyses.

2.3.6. Molecular Dynamics Simulation.
Molecular dynamics (MD) is an approximation of the behaviour of the system against real conditions and allows to test the stability of the ligand-protein contacts, which were detected during the BD and VS analyses, during a period of time.

MD simulations were carried out using the GPU version of Desmond included with Maestro suite 2019.4 (Schrödinger LLC) on a workstation with a NVIDIA QUADRO 5000. The system conformed by the ligand and protein of interest was solvated in an aqueous environment, in a cubic box with a minimal distance of 10 Å between the biomolecule and the box boundary (for periodic boundary conditions). Next, systems were neutralized and maintained in 0.15 M NaCl. The OPLS3 force field and the TIP3P-TIP4P water model were employed. Initially, the systems were simply energy-minimized for 2000 time steps. Next, systems were allowed to execute free dynamics in the NPT ensemble; pressure was controlled using the Martyna–Tobias–Klein methodology, and the Nose–Hoover thermostat was employed to maintain the system near 310K. Production-grade MD trajectories were extended to a total duration of 20 ns per system.

MD trajectories were characterized in terms of the root mean square deviation (RMSD) of fluctuations of ligand and receptor, particularly in terms of the main interactions with the top interacting residues. The trajectories were also used to assess the stabilities of the protein secondary structures (in complex with potential inhibitor) by plotting RMSDs.

2.4. In Vitro Assay

2.4.1. Spike-ACE2 Binding Assay.
The *in vitro* enzyme-linked immunosorbent assay is a sensitive method to characterize the binding of the spike-ACE2 complex in the presence of potential inhibitors. The assay uses a 96-well plate coated with recombinantly expressed receptor-binding domain (RBD) of the SARS-CoV-2 spike protein. The testing reagent-of-choice is then added to the wells in the presence of recombinant human ACE2 protein. Unbound ACE2 is removed by washing, and a goat anti-ACE2 antibody that binds to the spike-ACE2 complex is added.

HRP-conjugated anti-goat IgG is then applied to the wells in the presence of 3,3′, 5,5′-tetramethylbenzidine (TMB) substrate. The HRP-conjugated anti-goat IgG binds to the ACE2 antibody and reacts with the TMB solution, producing a blue colour that is proportional to the amount of bound ACE. The HRP-TMB reaction is halted with the addition of the stop solution, resulting in a blue-to-yellow colour change. The intensity of the yellow colour is then measured at 450 nm. The percentage of inhibition of the formation of the spike-ACE2 complex was calculated as follows:

$$\text{Spike} - \text{ACE2 binding inhibition}\,(\%) = \frac{A_{\text{control}} - A_{\text{sample}}}{A_{\text{control}}} \cdot 100,$$

$$(1)$$

where A_{control} is the absorbance without inhibitor (considered as 100% Spike-ACE2 binding) and A_{sample} is the absorbance of sample with inhibitor.

2.4.2. ACE2 Inhibitor Screening Assay.
The ACE2 inhibitor screening kit was used to detect potent inhibitors of ACE2 activity. It utilizes the ability of an active ACE2 to cleave a synthetic MCA-based peptide substrate to release a free fluorophore. The released MCA is easily quantified using a fluorescence microplate reader (excitation wavelength 320 nm and emission wavelength 420 nm). In the presence of an ACE2-specific inhibitor, the enzyme loses its peptidase activity which results in the decrease of fluorescence intensity. The ACE2 percentage inhibition was calculated as follows:

$$\text{ACE2 inhibition}\,(\%) = \frac{F_{\text{control}} - F_{\text{sample}}}{F_{\text{control}}} \cdot 100, \qquad (2)$$

where F_{control} is the fluorescence with ACE2 and without inhibitor (considered as 100% enzyme activity) and F_{sample} is the fluorescence of sample with ACE2 and inhibitor.

3. Results and Discussion

3.1. Molecular Docking and Virtual Screening.
Angiotensin-converting enzyme 2 is known to be one of the essential host receptors for SARS coronaviruses, and it is

also proved to be the major cellular receptor for the novel SARS-CoV-2. ACE2 is a membrane protein expressed in the lungs, kidneys, heart, and intestine, and it is responsible for vasoconstriction and blood pressure control, being its decreased expression associated with cardiovascular diseases.

COVID-19 disease causes ACE2 downregulation, affecting the tissues where it is expressed, but with major implications for lung and heart tissues, causing both pulmonary and cardiovascular complications [47, 48]. There are several studies that identify the region of interaction between the virus and this receptor, proving that the $\alpha 1$ and $\alpha 2$ helices are the most important areas of interaction [10–12]. Hence, the development of effective treatment should consider the blockage of this area to avoid SARS-CoV-2 binding, but the capacity for ACE2 expression enhancement should be also kept in mind.

ACE2 infection is caused due to the fusion between this enzyme and the spike glycoprotein of SARS-CoV-2. The S1 and S2 subunits of the spike are known to be responsible for the receptor binding (S1) and for the membrane fusion among the viral subunit and ACE2 (S2) [49].

The crystal structure between ACE2 and the spike glycoprotein is elucidated, and the residues which take part in the binding process are identified. To avoid virus infection, the blockage of the spike glycoprotein or the host cell receptors should be considered.

Similar to ACE2, dipeptidyl peptidase is considered an important entry receptor for SARS coronaviruses, including MERS-CoV, SARS-CoV, and SARS-CoV-2 [44, 50, 51].

CD26 has a key role in immune regulation as a T-cell activation molecule and in immune-mediated disorder, thus acting as a key immunoregulatory factor in viral infections. The S1 loop is considered to be the area of interaction of this receptor and SARS-CoV-2, being its key residues clearly identified, so therapies to overcome the COVID-19 can be developed by targeting this region [13].

As a SARS-CoV-2 host receptor, angiotensin-converting enzyme was also identified as an important target. ACE is the precursor of angiotensin II, which is a strong inducer of vascular smooth muscle cells (VSMCs) by activating the AT1 receptor. The VSMCs are essential to maintain vascular function and homeostasis, being its upregulation responsible for the overexpression of proinflammatory cytokines and growth factors as IL-6, IL-8, and NF-kB, among others [14].

Lungs are one of the most affected organs when the overexpression of the inflammatory cascade takes place. Accordingly, high inflammation levels are associated with major complications of COVID-19, so ACE inhibition may be a suitable strategy to avoid or mitigate this process [19, 20]. The ACE residue Glu384 is considered the key of the hot spot, so its regulation can be achieved by triggering this amino acid.

A different strategy to fight the COVID-19 infection can be the direct treatment of the virus. The viral protease 3CLpro has been proved to be essential for coronavirus replication and is thus considered the most potent drug target among the virus receptors [5, 9]. The dyad His41-Cys145 conforms the hot spot of this receptor, so an effective SARS-CoV-2 disabling can be developed by targeting these key residues.

To target these five receptors, the pea peptides, LSDRFS and SDRFSY, and the amaranth peptides, GGV, IGV, IVG, VGVL, and VIKP, are proposed. Its binding capacities are analysed in a docking study which detects, first, the regions of interaction of each peptide among the whole target receptor. This will indicate whether the peptide reaches the hot spot or remains trapped in ineffective areas of the protein.

Thereafter, these effective interactions are characterized in terms of affinity energy. The different types of interaction (hydrogen bond, hydrophobic interaction, π-π interaction, and salt bridge) between ligand and receptor will determine its magnitude giving an associated energy value or score. Hence, those ligands which reach the hot spot area with sufficient energy are susceptible of being effectively bound to the receptor, enhancing or inhibiting its associated biological activity.

3.1.1. Angiotensin-Converting Enzyme 2 (ACE2).

Angiotensin-converting enzyme 2 (ACE2) is considered one of the major host receptors of β-coronaviruses, including SARS-CoV, MERS-CoV, and SARS-CoV-2. Regarding the SARS-CoV-2, its interaction takes place among the $\alpha 1$ and $\alpha 2$ helices of ACE2, where residues Gln24, Asp30, His34, Tyr41, Gln42, Met82, Lys353, and Arg357 play a major role in reinforcing virus interaction [11, 12].

There is some controversy about the regulation of ACE2. Some authors indicate that ACE2 expression reduction could be beneficial, so the main host receptor for SARS-CoV-2 would be diminished, involving a less acute infection [52]. Nevertheless, this would cause an increase of the ratio Ang II:Ang 1–7, exacerbating the pulmonary tissue damage initially provoked by SARS-CoV-2 [47, 48, 53]. It is true that cardiovascular tissues or cells that express ACE2 are potentially at risk for SARS-CoV-2 infection; however, ACE2 expression reduction would be also detrimental.

The moderate enhancing production of ACE2 with a blocking agent, which helps to protect the area of interaction between ACE2 and SARS-CoV-2, may be a good approach to prevent COVID-19 disease while an adequate ratio Ang II:Ang 1-7 is maintained to avoid pulmonary tissue damage.

Several pea peptides had been proved to be bioactive against ACE2, so ligands as LSDRFS and SDRFSY are known to interact in the hot spot of this receptor [39]. Besides, it is well known that when a ligand shows bioactivity against one receptor, it would bind its hot spot but also other nonactive areas of the target. Thus, considering the key area of interaction of SARS-CoV-2 in ACE2, a blind docking analysis was performed to detect both the region of interaction and its magnitude for the pea peptides, LSDRFS and SDRFSY, and the amaranth peptides, GGV, IGV, IVG, VGVL, and VIKP.

Table 1 shows the global affinity values, calculated with AutoDock 4.2, and the affinities related to the key residues for virus interaction, calculated with PoseView 1.1.2.

Table 1: Angiotensin-converting enzyme 2 (ACE2) docking analysis.

Drug/peptide	E bond$_{global}$ (kcal/mol)	E bond$_{key\ residues}$ (kcal/mol)	Drug/peptide	E bond$_{global}$ (kcal/mol)	E bond$_{key\ residues}$ (kcal/mol)
	−7,98	>−2	IGV	−5,05	−2,557
Ritonavir (347980)	−5,86	−2,274 −2,080		−4,7	>−2
	−5,79	−2,279 −2,055 −2,313	IVG	−5,25	−3,559
	−5,88	−2,557		−4,88	−2,106
Lopinavir (83706)	−5,3	−2,903		−5,14	>−2
	−4,85	>−2	VGVL	−4,93	−4,000
Emtricitabine (54859)	−4,94	−5,184		−4,28	−5,587
	−4,83	−4,453	VIKP	−5,18	−2,049
Hydroxychloroquine (3526)	−5,06	>−2		−4,69	>−2
	−4,71	>−2		−4,66	−2,543
	−4,46	−3,965		−5,93	−4,115 −8,610
	−4,8	>−1	LSDRFS	−5,69	−5,649 −2,366 −2,557
Chloroquine (2618)	−4,39	>−2		−5,51	−2,351
	−4,18	>−2		−4,69	−11,390 −2,191
	−5,78	−4,866		−7,56	−5,494
GGV	−4,76	−2,557	SDRFSY	−6,32	−2,759 −2,352 −4,389
	−4,32	−3,576		−6,05	−6,452

LSDRFS and SDRFSY show the best performance against ACE2 (Table 1), even compared to drugs that were studied for drug repositioning such as ritonavir, lopinavir, emtricitabine, hydroxychloroquine, or chloroquine [54–56]. Regarding the global interaction energy, SDRFSY has a better affinity value. Nevertheless, the ACE2 key residues that are fundamental for virus infection (Figure 1, yellow colour) are more strongly bound to LSDRFS than to SDRFSY. This means that these positions would be involved in the LSDRFS interaction, blocking the access of the SARS-CoV-2 to this area (Figure 1).

Comparing the area of interaction of these two peptides, LSDRFS covers a more extensive area of the hot spot region than SDRFSY. There are four positions of interaction that are involved with key residues (Figure 1(a)), and SDRFSY peptides let exposed the key residues Tyr41 and Lys353, located at the left side of $\alpha2$ helix, and Gln24 and Met82, located at the right side of both helixes. Thus, due to the stronger interactions and larger blocked area, LSDRFS is expected to be more effective than SDRFSY to prevent ACE2 infection.

VGVL and VIKP also show good global affinity values, but only two positions of the key binding area are effectively blocked (Supplementary Figures 29 and 33), within key residue energies lower than −2.00 kcal/mol (Supplementary Figures 30 and 36), so this would probably cause poor blocking capacity against SARS-CoV-2 infection.

GGV also shows a good performance, regarding the global and key residue energies, but the small size of this amaranth peptide does not allow to cover the whole area where the virus interacts (Figure 1(c)). However, the combination of GGV and LSDRFS can be a promising match. Figure 1(d) shows that there are no competitive interactions between these ligands, so they interact along the whole $\alpha1$ and $\alpha2$ helices covering the main area of virus interaction and matching their strong binding capacities. This LSDRFS-GGV combination may be the most promising strategy to protect ACE2 from SARS-CoV-2 infection.

3.1.2. Spike Glycoprotein. The spike glycoprotein or S protein of coronaviruses, including SARS-CoV-2, is one of their most important structural proteins. It recovers the external capsid of the virion, giving the appearance of a crown. Conformed by three major sections, ectodomain, single-pass transmembrane, and intracellular tail, the most important one is the ectodomain. This section is divided in two different subunits: the S1, responsible for the receptor binding to the host cells, and the S2, the membrane fusion unit [40, 49, 50].

The main host receptor for SARS-CoV-2 and thus spike glycoprotein is ACE2. Several studies had identified the residues that take part in this interaction, revealing the importance of Tyr449, Tyr453, Leu455, Phe456, Phe486, Asn487, Tyr489, Gln493, Gly496, Gln498, Thr500, Asn501, Gly502, and Tyr505 [41, 51].

Blind docking and virtual screening analyses were performed to detect the possible interactions between spike glycoprotein and the amaranth peptides, GGV, IGV, IVG, VGVL, and VIKP, and the pea peptides, LSDRFS and SDRFSY (Supplementary Table 1, Supplementary Figures 44–64). Regarding the affinity scores (Supplementary Table 1), it seems that these ligands are not suitable to shield the crown of the SARS-CoV-2 and prevent an infection (Supplementary Figures 44–64). Nevertheless, this can be considered as a beneficial behaviour. It is well known that a certain molecule can act as a protein-protein stabilizer, enhancing the interaction between two (or more) different proteins [57]. This ineffective interaction with the protein S proves that there is no possibility for these peptides to enhance the ACE2 infection, so these results reinforce the promising behaviour of LSDRFS, SDRFSY, and the combination LSDRFS-GGV against ACE2 host receptor.

3.1.3. Cluster of Differentiation 26 (CD26). The cluster of differentiation 26 (CD26), also known as dipeptidyl peptidase, has been recognized as an important host receptor of
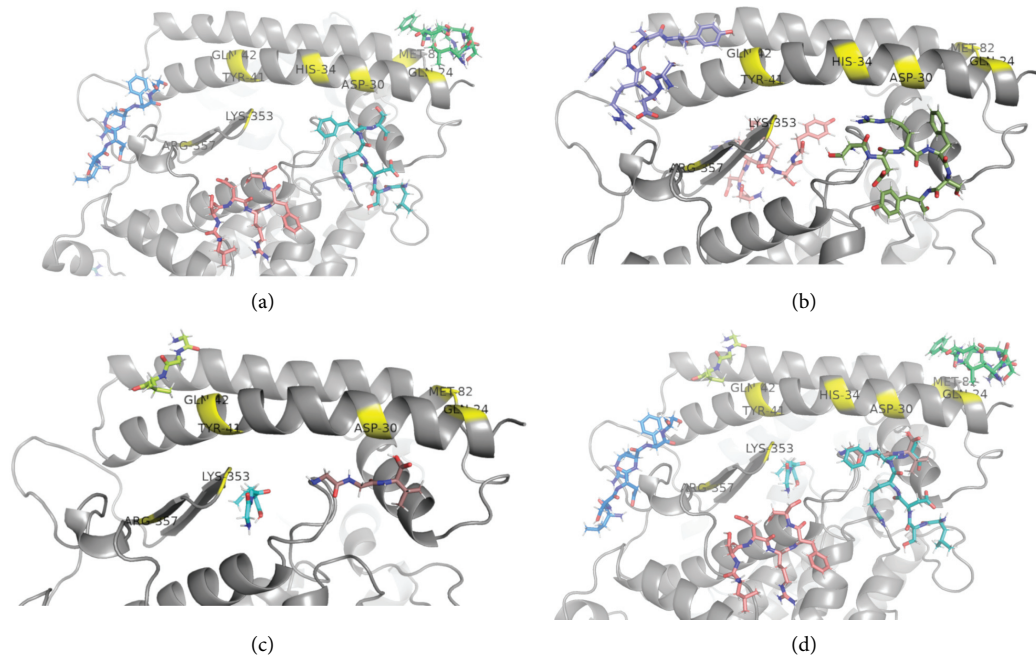
(a)

(b)

(c)

(d)

FIGURE 1: Angiotensin-converting enzyme 2 blind docking analysis. (a) LSDRFS, (b) SDRFSY, (c) GGV, and (d) LSDRFS and GGV. Yellow = hot spot area/key residues. ACE2 PBD: 6m18.

SARS-CoV-2. Residues Lys267, Gln286, Ile287, Thr288, Ala289, Ala291, Leu294, Ile295, Arg317, Tyr322, Arg336, and Asn338 from S1 loop were identified as key residues in virus interaction [13].

A blind docking analysis was performed to detect the possible interactions between this receptor and the proposed ligands LSDRFS, SDRFSY, GGV, IGV, IVG, VGVL, and VIKP. Also, the approved drugs chloroquine, hydroxy-chloroquine, and ritonavir, studied for drug repurposing, were tested following the same procedure. Accordingly, peptide and drug results can be compared (Supplementary Table 2, Supplementary Figures 65–74), showing similar responses for SDRFSY and hydroxychloroquine, with high-affinity values against CD26.

The hydroxychloroquine exerts a good performance against CD26, with great binding energies and blocking Val341, Asn338, Arg336, Gln286, and Lys287 from virus interaction (Supplementary Figure 66, Supplementary Table 2). Nevertheless, the central area conformed by residues Ala291, Tyr322, Leu294, Ile295, and Arg317 is uncovered, exposing important residues from the hot spot and allowing the virus binding. SDRFSY performance can be compared with the hydroxychloroquine (Supplementary Figure 74, Supplementary Table 2), so it has also good energy values for global and key residues interaction. Due to the size of this pea peptide, a broad area of CD26 is expected to be inhibited, so Supplementary Figure 74 shows almost a total binding of the hot spot, being only Tyr322 and Arg336 unbound. This would help to protect the receptor against virus entry. Regarding the other studied drugs and peptides, low binding capacities are detected, so they are not expected to be effective virus blockers (Supplementary Table 2, Supplementary Figures 65–74).

3.1.4. Angiotensin-Converting Enzyme (ACE). Angiotensin-converting enzyme was selected as target because of its connexion to the inflammatory process mediated by NF-kB transcription factor, which is overexpressed in patients with major COVID-19 complications.

Several pea and amaranth peptides are proved to have ACE inhibitory capacity, so LSDRFS, SDRFSY, GGV, IGV, IVG, VGVL, and VIKP ligands are studied against ACE by means of blind docking and virtual screening analyses. Also, the approved drug captopril was tested following the same procedure to contrast drug and peptide results (Supplementary Table 3, Supplementary Figures 75–90).

Glu384 is considered by UniProtKB database as the key residue to inhibit the hypertension effect caused by ACE. Supplementary Table 3 summarizes the global and key residue binding energies of the proposed drugs and peptides, showing that LSDRFS and VIKP are expected to behave as effective hypertension reduction agents, thus also helping to reduce the inflammation levels of the organism. IGV and VGVL show also great inhibitory potentials, being only GGV results below captopril ones (Supplementary Figures 75–90). This is an indication of the angiotensin reduction capacity of these peptides, which may be suitable to inhibit the NF-kB transcription factor overexpression while helping to block the area of interaction of ACE2 and SARS-CoV-2. Hence, peptides as LSDRFS, with favourable binding capacities against ACE2 and ACE, are expected to exert a double action against COVID-19.

3.1.5. Chymotrypsin-Like Protease (3CLpro). The chymotrypsin-like protease enzyme (3CLpro) is indispensable to the viral replication and infection process, so it is considered
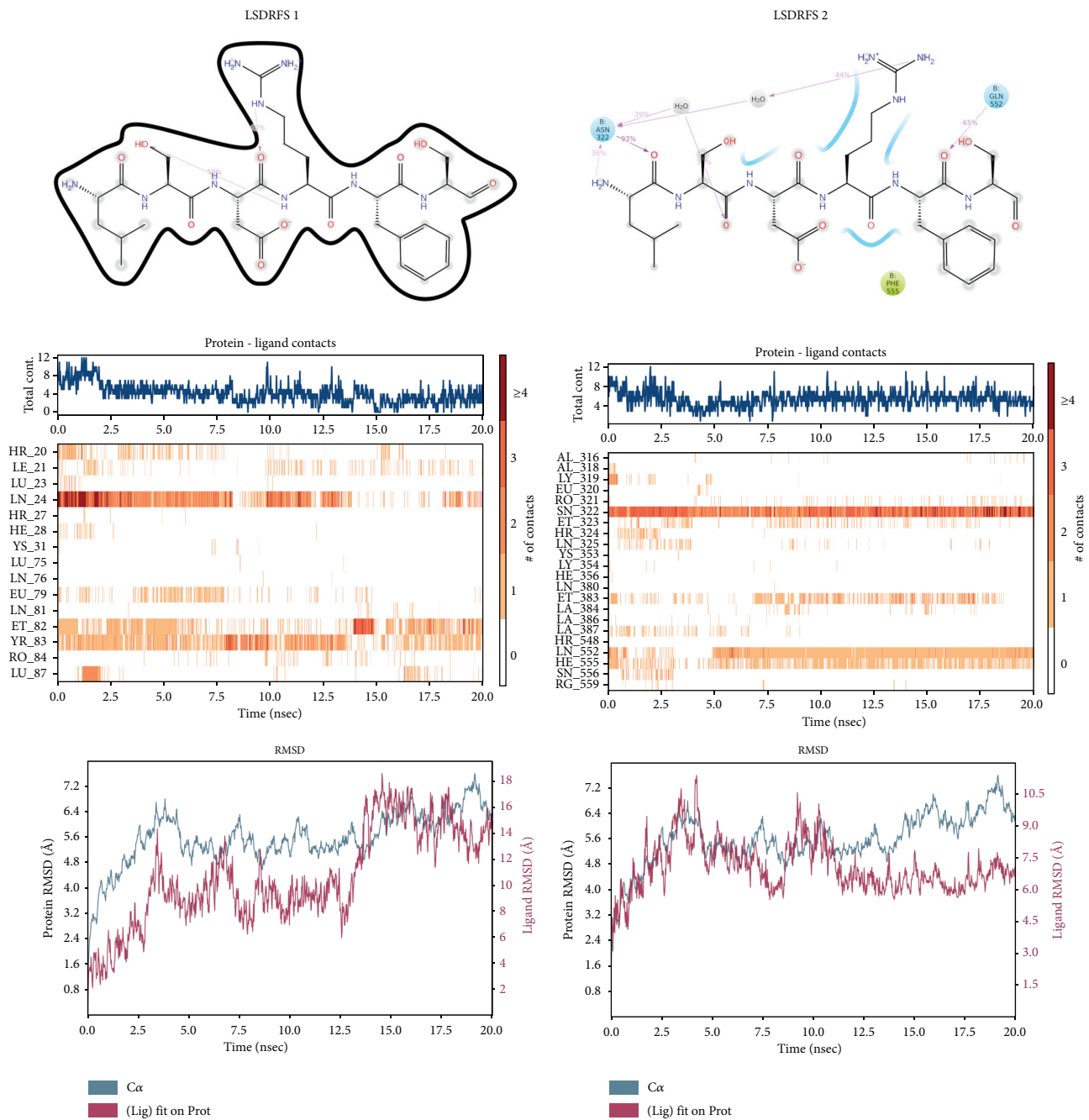
Figure 2: Molecular dynamics simulation LSDRFS-ACE2. Analysis of positions 1 and 2: interactions and RMSD fluctuation.

nowadays the most important target to develop an antiviral therapy [9]. Several approved drugs are being studied for drug repositioning by targeting this receptor, such as demeclocycline, doxycycline, oxytetracycline, lymecycline, nicardipine, telmisartan, and conivaptan [5].

It is unlikely that the proposed peptides would bind and inhibit 3CLpro, but due to the favourable binding of some of these ligands with ACE and ACE2, it is important to test their possible interferences with the virus itself. The hot spot of the 3CLpro receptor is the catalytic dyad His41-Cys145 [5, 9]. Thus, blind docking and virtual screening analyses were performed for 3CLpro and peptides LSDRFS, SDRFSY, GGV,

IGV, IVG, VGVL, and VIKP regarding this binding site. Also, demeclocycline, doxycycline, oxytetracycline, lymecycline, nicardipine, telmisartan, and conivaptan are studied following the same procedure to contrast drug and peptide results (Supplementary Table 4, Supplementary Figures 91–103).

The poor bond energies of this analysis suggest, as it was expected, an ineffective interaction between these ligands and the 3CLpro virus receptor results (Supplementary Table 4, Supplementary Figures 91–103). However, this noninteraction between peptides and the main virus receptor can be favourable because it proves that there is no possibility of these peptides to act as a protein–protein stabilizer, enhancing the interaction

Figure 3: Molecular dynamics simulation LSDRFS–ACE2. Analysis of positions 3 and 4: interactions and RMSD fluctuation.

between two (or more) different proteins [57]. Hence, these peptides are well-suited to inhibit the regions of interaction of ACE2 (LSDRFS and SDRFSY peptides) and mitigate the inflammation process by triggering ACE (LSDRFS and VIKP peptides) without exerting an attraction effect against the 3CLpro nor the spike protein SARS-CoV-2 receptors.

3.2. Molecular Dynamics Simulation. Molecular dynamics simulation study was performed to test the stability of the interactions detected during the molecular blind docking

and virtual screening analyses. The LSDRFS, SDRFSY, and VIKP–ACE2 systems were studied following this protocol. Also, hydroxychloroquine was submitted to the same process to contrast peptide and drug performances [54]. Each ligand interaction with ACE2 was analysed, reporting the main protein-interacting residues during the simulation period and its correspondent RMSD plots (Figures 2–5, Supplementary Figures 104 and 105).

The first docking position of LSDRFS (Figure 2) shows a persistent interaction with Gln24 during the first 10 ns, but it becomes unstable after that, and a more intermittent but
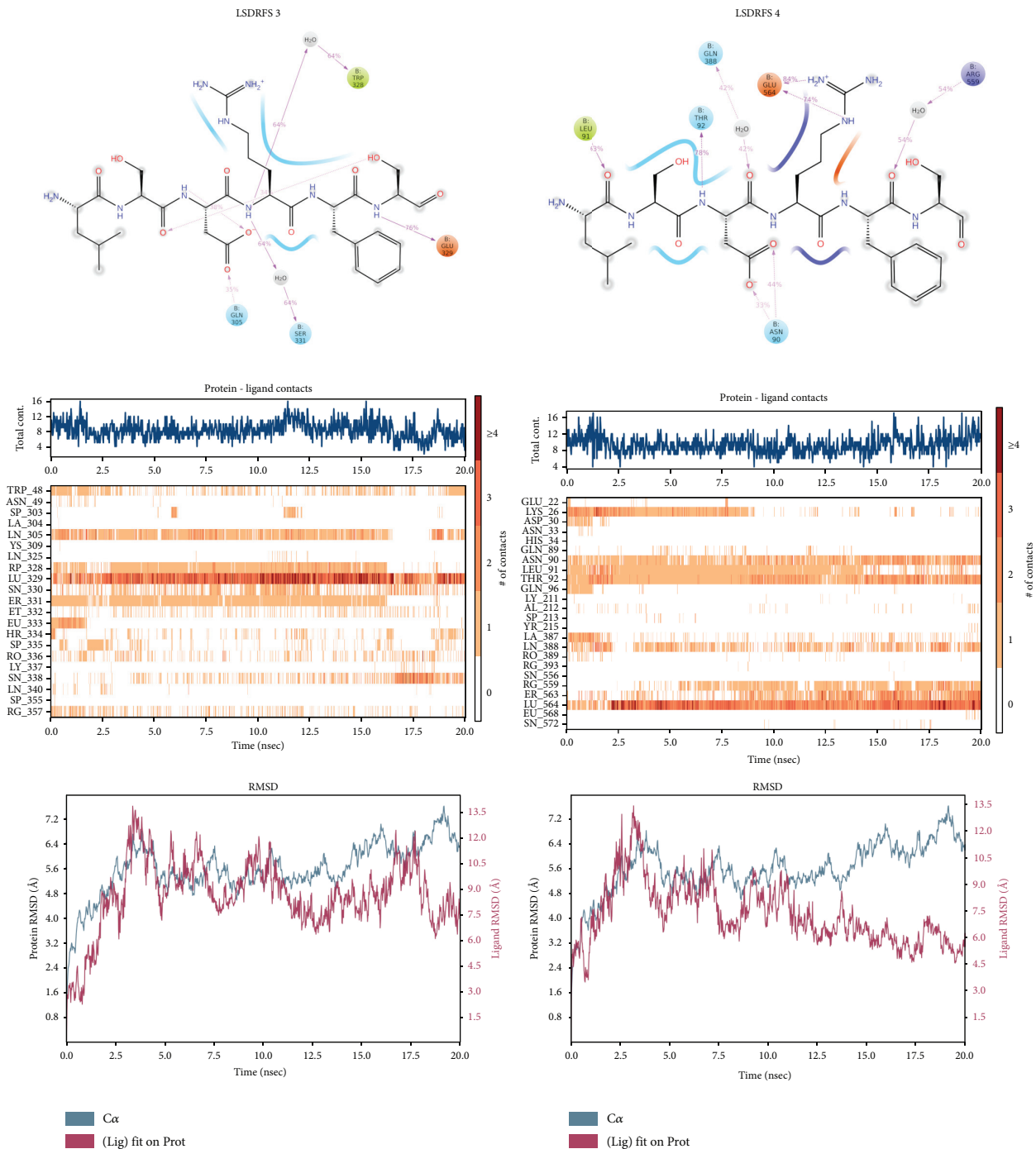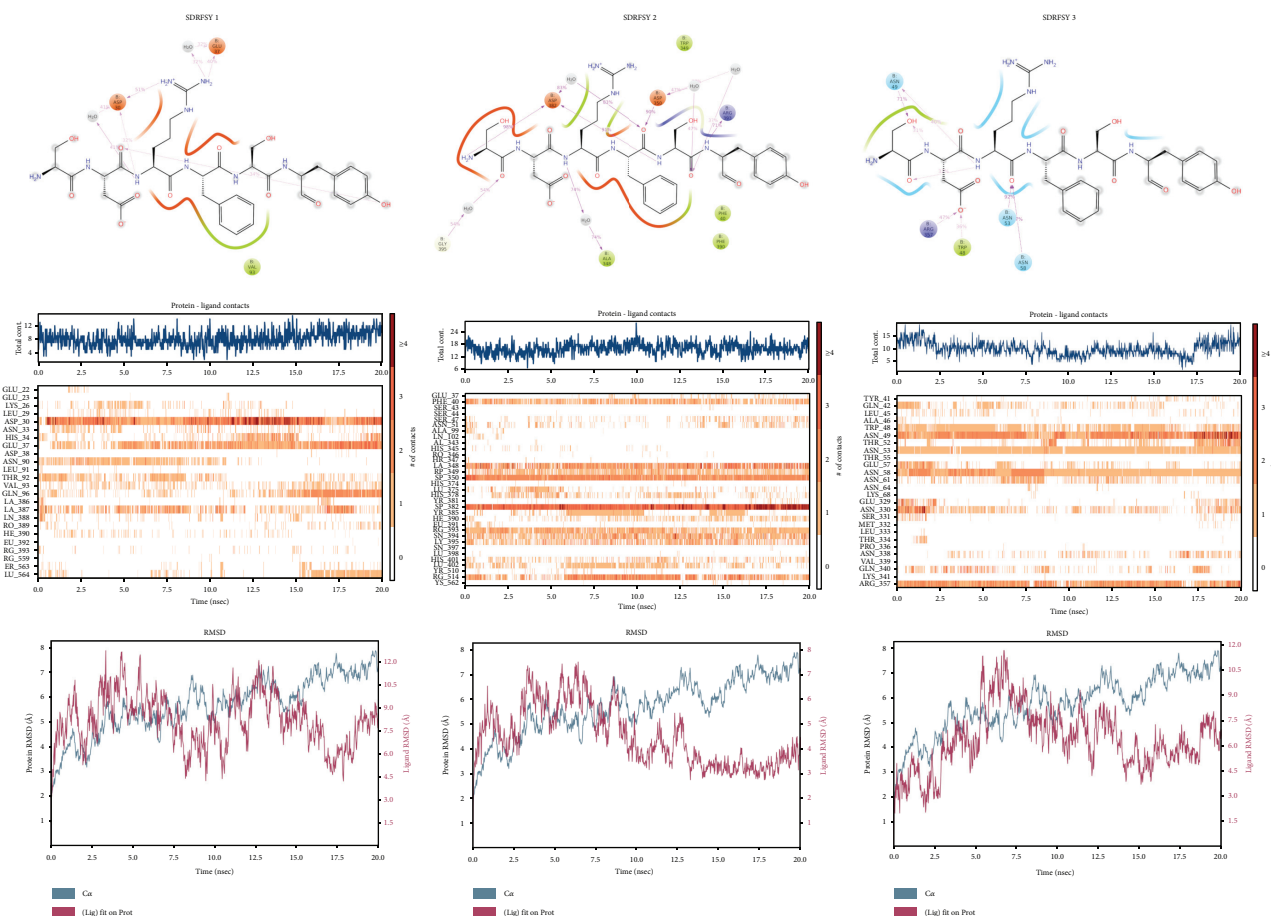
FIGURE 4: Molecular dynamics simulation SDRFSY-ACE2. Analysis of positions 1, 2, and 3: interactions and RMSD fluctuation.

stable interaction with Met82. There are no persistent contacts during the whole simulation, so this is translated to the RMSD values, which show a high value around 18 Å. The second docking position (Figure 2) interacts persistently with Asn322 and Gln552, and more intermittently but stably with Phe555. This position is maintained during the whole simulation, causing lower and stable RMSD values (around 7 Å). Furthermore, the peptide head and tail are involved in these interactions, fixing the whole position of this peptide and thus blocking a wide area which otherwise would be available for spike glycoprotein reception.

A quite similar behaviour is present at the third docking position (Figure 3), which has stable interactions with Gln305, Trp328, and Ser331 and a persistent interaction with Glu329. Accordingly, the RMSD values are moderate and stable around 8 Å. The fourth position analysis (Figure 3) reveals persistent interactions with Asn90, Thr92, and Glu564 and high stable interactions with Leu91, Gln388, Arg559, and Ser563. This is translated to the RMSD value, which is stable and low (around 6 Å). The whole structure of this peptide (head, centre, and tail) is well fixed to the protein, causing a high stable interaction and allowing to block a big area where the spike glycoprotein interacts.

LSDRFS shows stable interactions with ACE2, specially the second and fourth positions, followed by the third one (Figures 2 and 3). This is expected to efficiently block the

virus entry by covering an important area where the spike glycoprotein causes the ACE2 infection (Figure 1(a)).

The first docking position of SDRFSY shows a persistent interaction with Asp30 and high stable interactions both with Glu37 and Ala387. Also, it has more intermittent but stable interactions with Val93 and Gln96 (Figure 4). The peptide is fixed to the protein in its central zone, leaving the head and tail amino acids free to rotate. This makes the RMSD values slightly high (around 8.5 Å), but still covers a large area of the protein in a stable way. The second position (Figure 4) shows persistent interactions with Phe40, Ala348, Trp349, Asp350, Asp382, Arg393, Asn394, and Gly395 and also stable but slightly more intermittent interactions with Phe390, His401, and Arg514. This high number of contacts makes the peptide interaction very stable, with RMSD values around 4 Å. In addition, the whole peptide structure is bound to the protein, covering a large area of the protein in a very stable way, so a high capacity to prevent virus binding is expected. The third position (Figure 4) has persistent interactions with Trp48, Asn49, Asn53, Asn59, and Arg357. It also interacts slightly more intermittently with Asn61 and Asn330. The head amino acids are specially well fixed to the protein (Figure 4), leaving the tail free to rotate, which causes mid-low RMSD values around 7 Å.

SDRFSY shows three interactions along the area of interaction of ACE2 and spike glycoprotein (Figure 1(b)).
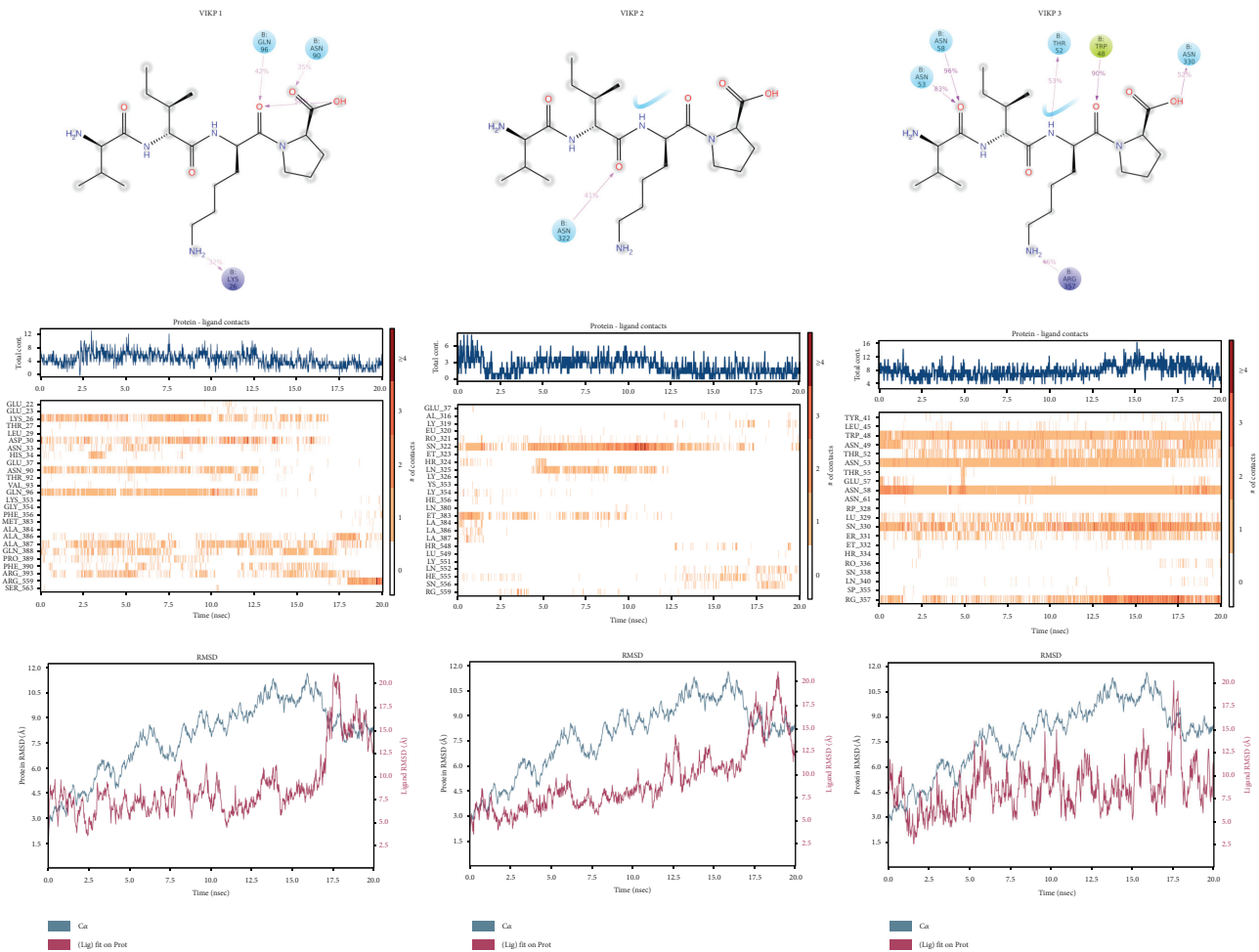
Figure 5: Molecular dynamics simulation VIKP–ACE2. Analysis of positions 1, 2, and 3: interactions and RMSD fluctuation.

These three docking positions have a high number of persistent contacts with ACE2 (Figure 4), making SDRFSY interactions very stable and thus preventing virus binding by covering its main area of interaction.

VIKP shows intermittent and unstable interactions for the first and second docking positions (Figure 5), with high RMSD values around 12 Å. Only the third position is considered stable, so it has persistent interactions with Trp48, Asn53, and Asn58 and low RMSD values around 4 Å (Figure 5).

Blind docking and virtual screening analyses reveal VIKP as a weaker candidate for ACE2 binding. This was also proved by molecular dynamics analysis (Figure 5), which show intermittent and unstable interactions specially for the first and second docking positions. Despite the stable interaction of the third position, the small size of this peptide does not allow to cover a large area of ACE2, so it is not expected to act as spike glycoprotein blocker.

The high number of persistent contacts and low RMSD values of SDRFSY show the high stability of SDRFSY–ACE2 interactions, so this peptide is expected to behave as a good inhibitor for spike glycoprotein binding, followed by LSDRFS, with slightly higher instability but also strong interactions with several ACE2 key residues.

These molecular dynamics results were compared with hydroxychloroquine, showing a better performance to prevent the virus infection than this drug which was used for COVID-19 treatment (Supplementary Figures 104 and 105), so SDRFSY and LSDRFS peptides are potential candidates to act preventively against mid SARS-CoV-2 infection.

3.3. In Vitro Assays. The in vitro analyses were carried out following the fluorimetric procedure explained before. The percentages of inhibition of peptides LSDRFS, SDRFSY, VIKP, and GGV for spike glycoprotein-ACE2 interaction and ACE2 activity are shown in Table 2.

SDRFSY and LSDRFS show a higher inhibitory potential at spike–ACE2 and also ACE2 analysis. This is an indicative of the strong interaction of these peptides within the ACE2 receptor, which would prevent virus (spike glycoprotein) and host (ACE2) from forming an effective interaction. This is in accordance with the results obtained by the computational method, which predicted a good performance for SDRFSY and LSDRFS (Table 1, Figures 1–4).

VIKP shows lower inhibition values, as it was also reported by the docking and molecular dynamics analyses (Table 1, Figure 5). However, results for the combination of

TABLE 2: Inhibitory effects of peptides on the interaction between SARS-CoV-2 spike glycoprotein and the human ACE2 receptor and on the ACE2 activity. a = 15 g/L, b = 7.5 g/L, c = 15 g/L (1 : 1), and d = 15 g/L (2 : 1), n.d. = not detected.

Peptides	Spike-ACE2			ACE2	
	PI (%)[a]	PI (%)[c]	PI (%)[d]	PI (%)[a]	PI (%)[b]
LSDRFS	79.56	—	—	95.50	52.17
SDRFSY	84.65	—	—	95.81	71.33
VIKP	62.03	—	—	94.37	16.4
GGV	34.99	—	—	6.07	n.d
LSDRFS + GGV	—	4.08	38.29	—	—

LSDRFS and GGV widely differ from the molecular modelling ones, which foresaw a synergetic effect for the combination of these peptides (Figure 1(d)). This is probably due to the incorrect positioning of the peptides in the interaction zone of ACE2 and spike glycoprotein. Although after the BD analysis these ligands were located at compatible poses and positions, avoiding binding competition between them, regarding the obtained results, GGV probably presents a higher instability that interferes with LSDRFS interaction positions, causing poor inhibition capacities.

4. Conclusions

β-Coronaviruses have crossed the animal–human barrier, causing several outbreaks during recent years, but none of them with the dimensions of SARS-CoV-2, which has been spread for over the world [58], so both treatment and preventive approaches are urgently required. In this scenario, natural peptides play a major role offering a preventive strategy or a treatment for nonacute patients due to its GRAS (generally recognised as safe) property.

In this study, several pea and amaranth peptides were analysed against the major SARS-CoV-2 receptors—both host and virus. Molecular docking and dynamics simulation results show that SDRFSY and LSDRFS have strong and stable interactions with ACE2, so these peptides can be suitable to shield the area of ACE2 where the spike glycoprotein of the virus exerts its interaction (Table 1, Figures 1(a) and 1(b)). It was also proved that none of the studied peptides interacts with the spike glycoprotein, so their presence does not cause an increase in the interactions between ACE2 and the spike glycoprotein, which verifies that these peptides do not have the potential to act as protein–protein interaction (PPI) stabilizers (Supplementary Table 2). These theoretical results were confirmed by *in vitro* analyses, proving that SDRFSY and LSDRFS prevent the spike glycoprotein–ACE2 interaction with inhibition percentages above 80% at 15 g/L (Table 2).

Also, computational results show that CD26 can be similarly protected with SDRFSY and VIKP (Supplementary Table 2), and ACE, which is inextricably linked to the cytokine cascade that causes major complications in acute COVID-19 patients, can be inhibited by LSDRFS and VIKP (Supplementary Table 3).

Hence, it can be assessed that the pea peptides, SDRFSY and LSDRFS, and the amaranth peptide, VIKP, are susceptible of being useful not to overcome but to mitigate and prevent the effects of the SARS-CoV-2 in an effective and quick manner.

Data Availability

The data used to support the findings of this study are included within the supplementary information file.

Conflicts of Interest

The authors declare that there are no conflicts of interest related to this publication.

Supplementary Materials

Blind docking and virtual screening analyses of spike glycoprotein, cluster of differentiation 26 (CD26), angiotensin-converting enzyme (ACE), and 3-chymotrypsin-like protease enzyme (3CLpro). (*Supplementary Materials*)

References

[1] G. Viceconte and N. Petrosillo, "COVID-19 R0: magic number or conundrum?" *Infectious Disease Reports*, vol. 12, pp. 12-13, 2020.

[2] Y. Liu, A. A. Gayle, A. Wilder-Smith, and J. Rocklöv, "The reproductive number of COVID-19 is higher compared to SARS coronavirus," *Journal of Travel Medicine*, vol. 27, no. 2, pp. 1–4, 2020.

[3] K. F. Amanat Fatima, "SARS-CoV-2 vaccines: status report," *Cell*, vol. 52, no. 4, pp. 1–7, 2020.

[4] M. Wang, R. Cao, L. Zhang et al., "Remdesivir and chloroquine effectively inhibit the recently emerged novel coronavirus (2019-nCoV) in vitro," *Cell Research*, vol. 30, no. 3, pp. 269–271, 2020.

[5] C. Wu, Y. Liu, Y. Yang et al., "Analysis of therapeutic targets for SARS-CoV-2 and discovery of potential drugs by computational methods," *Acta Pharmaceutica Sinica B*, vol. 10, 2020.

[6] Y. Wang, D. Zhang, P. G. Du et al., "Remdesivir in adults with severe COVID-19: a randomised, double-bind, placebo-controlled, multicentre trial," *Lancet*, vol. 6736, no. 20, pp. 1–10, 2020.

[7] M. Koromina, M.-T. Pandi, and G. P. Patrinos, "Rethinking drug repositioning and development with artificial intelligence, machine learning, and omics," *OMICS: A Journal of Integrative Biology*, vol. 23, no. 11, pp. 539–548, 2019.

[8] K. H. Roux, S. S. Teuber, and S. K. Sathe, "Tree nut allergens," *International Archives of Allergy and Immunology*, vol. 131, no. 4, pp. 234–244, 2003.

[9] T. Pillaiyar, M. Manickam, V. Namasivayam, Y. Hayashi, and S.-H. Jung, "An overview of severe acute respiratory syndrome-coronavirus (SARS-CoV) 3CL protease inhibitors: peptidomimetics and small molecule chemotherapy," *Journal of Medicinal Chemistry*, vol. 59, no. 14, pp. 6595–6628, 2016.

[10] Y. Chen, Y. Guo, Y. Pan, and Z. J. Zhao, "Structure analysis of the receptor binding of 2019-nCoV," *Biochemical and Biophysical Research Communications*, vol. 525, no. 1, pp. 135–140, 2020.

[11] R. Yan, Y. Zhang, Y. Li, L. Xia, Y. Guo, and Q. Zhou, "Structural basis for the recognition of the SARS-CoV-2 by full-length human ACE2," *Science*, vol. 2762, pp. 1–10, 2020.

[12] J. S. Morse, T. Lalonde, S. Xu, and W. R. Liu, "Learning from the past: possible urgent prevention and treatment options for severe acute respiratory infections caused by 2019-nCoV," *ChemBioChem*, vol. 21, no. 5, pp. 730–738, 2020.

[13] N. Vankadari and J. A. Wilce, "Emerging COVID-19 coronavirus: glycan shield and structure prediction of spike glycoprotein and its interaction with human CD26," *Emerging Microbes & Infections*, vol. 9, no. 1, pp. 601–604, 2020.

[14] M. Suski, A. Gębska, R. Olszanecki et al., "Influence of atorvastatin on angiotensin I metabolism in resting and TNF-α -activated rat vascular smooth muscle cells," *Journal of the Renin-Angiotensin-Aldosterone System*, vol. 15, no. 4, pp. 378–383, 2014.

[15] W. Zhang, Y. Zhao, F. Zhang et al., "The use of anti-inflammatory drugs in the treatment of people with severe coronavirus disease 2019 (COVID-19): the experience of clinical immunologists from China," *Clinical Immunology*, vol. 214, Article ID 108393, 2020.

[16] T. Liu, L. Zhang, D. Joo, and S. C. Sun, "NF-κB signaling in inflammation," *Signal Transduction and Targeted Therapy*, vol. 2, 2017.

[17] T. Skurk, V. Van Harmelen, and H. Hauner, "Angiotensin II stimulates the release of interleukin-6 and interleukin-8 from cultured human adipocytes by activation of NF-κB," *Arteriosclerosis, Thrombosis, and Vascular Biology*, vol. 24, no. 7, pp. 1199–1203, 2004.

[18] D. Fliser, K. Buchholz, and H. Haller, "Antiinflammatory effects of angiotensin II subtype 1 receptor blockade in hypertensive patients with microinflammation," *Circulation*, vol. 110, no. 9, pp. 1103–1107, 2004.

[19] U. Kostakoglu, A. Topcu, M. Atak, L. Tumkaya, T. Mercantepe, and H. A. Uydu, "The protective effects of angiotensin-converting enzyme inhibitor against cecal ligation and puncture-induced sepsis via oxidative stress and inflammation," *Life Science*, vol. 241, Article ID 117051, 2020.

[20] R. Kranzhöfer, J. Schmidt, C. A. Pfeiffer, S. Hagl, P. Libby, and W. Kübler, "Angiotensin induces inflammatory activation of human vascular smooth muscle cells," *Arteriosclerosis, Thrombosis, and Vascular Biology*, vol. 19, no. 7, pp. 1623–1629, 1999.

[21] S. Puertas-Martín, A. J. Banegas-Luna, M. Paredes-Ramos et al., "Is high performance computing a requirement for novel drug discovery and how will this impact academic efforts?" *Expert Opinion on Drug Discovery*, vol. 15, no. 9, pp. 981–986, 2020.

[22] N. M. O'Boyle, M. Banck, C. A. James, C. Morley, T. Vandermeersch, and G. R. Hutchison, "Open babel: an open chemical toolbox," *Journal of Cheminformatics*, vol. 3, no. 10, pp. 1–14, 2011.

[23] A. W. Sousa Da Silva and W. F. Vranken, "Acpype-—AnteChamber PYthon parser interfacE," *BMC Research Notes*, vol. 5, pp. 1–8, 2012.

[24] S. Pronk, S. Páll, R. Schulz et al., "Gromacs 4.5: a high-throughput and highly parallel open source molecular simulation toolkit," *Bioinformatics*, vol. 29, no. 7, pp. 845–854, 2013.

[25] H. J. C. Berendsen, D. van der Spoel, and R. van Drunen, "GROMACS: a message-passing parallel molecular dynamics implementation," *Computer Physics Communications*, vol. 91, no. 1–3, pp. 43–56, 1995.

[26] C. Kutzner, S. Páll, M. Fechner, A. Esztermann, B. L. Groot, and H. Grubmüller, "More bang for your buck: improved use of GPU nodes for GROMACS 2018," *Journal of Computational Chemistry*, vol. 40, no. 27, pp. 2418–2431, 2019.

[27] E. F. Pettersen, T. D. Goddard, C. C. Huang et al., "UCSF chimera? a visualization system for exploratory research and analysis," *Journal of Computational Chemistry*, vol. 25, no. 13, pp. 1605–1612, 2004.

[28] G. M. Morris, R. Huey, W. Lindstrom et al., "AutoDock4 and AutoDockTools4: automated docking with selective receptor flexibility," *Journal of Computational Chemistry*, vol. 30, no. 16, pp. 2785–2791, 2009.

[29] O. Trott and A. Olson, "Autodock vina: improving the speed and accuracy of docking," *Journal of Computational Chemistry*, vol. 31, no. 2, pp. 455–461, 2010.

[30] P. C. D. Hawkins, A. G. Skillman, G. L. Warren, B. A. Ellingson, and M. T. Stahl, "Conformer generation with OMEGA: algorithm and validation using high quality structures from the protein databank and cambridge structural database," *Journal of Chemical Information and Modeling*, vol. 50, no. 4, pp. 572–584, 2010.

[31] S. Salentin, S. Schreiber, V. J. Haupt, M. F. Adasme, and M. Schroeder, "PLIP: fully automated protein-ligand interaction profiler," *Nucleic Acids Research*, vol. 43, no. W1, pp. W443–W447, 2015.

[32] A. Arnoldi, L. Carmen, and G. Aiello, "Cholesterol-reducing foods: proteins and peptides," *Encyclopedia of Food Chemistry*, vol. 3, pp. 323–329, 2018.

[33] R. Soares, S. Mendonça, L. Í. de Castro, A. Menezes, and J. Arêas, "Major peptides from Amaranth (*Amaranthus cruentus*) protein inhibit HMG-CoA reductase activity," *International Journal of Molecular Sciences*, vol. 16, no. 2, pp. 4150–4160, 2015.

[34] A. V. Quiroga, P. Aphalo, A. E. Nardo, and M. C. Añón, "In vitro modulation of renin-angiotensin system enzymes by amaranth (amaranthus hypochondriacus) protein-derived peptides: alternative mechanisms different from ACE inhibition," *Journal of Agricultural and Food Chemistry*, vol. 65, no. 34, pp. 7415–7423, 2017.

[35] A. Ayala-Niño, G. M. Rodríguez-Serrano, R. Jiménez-Alvarado et al., "Bioactivity of peptides released during lactic fermentation of amaranth proteins with potential cardiovascular protective effect: an in vitro study," *Journal of Medicinal Food*, vol. 22, pp. 1–6, 2019.

[36] A. Montoya-Rodríguez, M. A. Gómez-Favela, C. Reyes-Moreno, J. Milán-Carrillo, and E. González de Mejía, "Identification of bioactive peptide sequences from amaranth (*Amaranthus hypochondriacus*) seed proteins and their potential role in the prevention of chronic diseases," *Comprehensive Reviews in Food Science and Food Safety*, vol. 14, no. 2, pp. 139–158, 2015.

[37] B. Vecchi and M. C. Añón, "ACE inhibitory tetrapeptides from *Amaranthus hypochondriacus* 11S globulin," *Phytochemistry*, vol. 70, no. 7, pp. 864–870, 2009.

[38] G. Boschin, G. M. Scigliuolo, D. Resta, and A. Arnoldi, "ACE-inhibitory activity of enzymatic protein hydrolysates from lupin and other legumes," *Food Chemistry*, vol. 145, pp. 34–40, 2014.

[39] W. Liao, H. Fan, P. Liu, and J. Wu, "Identification of angiotensin converting enzyme 2 (ACE2) up-regulating peptides from pea protein hydrolysate," *Journal of Functional Foods*, vol. 60, Article ID 103395, 2019.

[40] I. Astuti and Ysrafil, "Severe acute respiratory syndrome coronavirus 2 (SARS-CoV-2): an overview of viral structure and host response," *Diabetes & Metabolic Syndrome: Clinical Research Reviews*, vol. 14, no. 4, pp. 407–412, 2020.

[41] D. Wrapp, N. Wang, K. S. Corbett et al., "Cryo-EM structure of the 2019-nCoV spike in the prefusion conformation," *Science*, vol. 367, no. 6483, pp. 1260–1263, 2020.

[42] V. Kumar, K.-P. Tan, Y.-M. Wang, S.-W. Lin, and P.-H. Liang, "Identification, synthesis and evaluation of SARS-CoV and MERS-CoV 3C-like protease inhibitors," *Bioorganic & Medicinal Chemistry*, vol. 24, no. 13, pp. 3035–3042, 2016.

[43] M. Letko, A. Marzi, and V. Munster, "Functional assessment of cell entry and receptor usage for SARS-CoV-2 and other lineage B betacoronaviruses," *Nature Microbiology*, vol. 5, 2020.

[44] G. Lu, Y. Hu, Q. Wang et al., "Molecular basis of binding between novel human coronavirus MERS-CoV and its receptor CD26," *Nature*, vol. 500, no. 7461, pp. 227–231, 2013.

[45] R. Strollo and P. Pozzilli, "DPP4 inhibition: preventing SARS-CoV-2 infection and/or progression of COVID-19?" *Diabetes/Metabolism Research and Reviews*, vol. 36, no. 1, 2020.

[46] A. Tapia-Abellán, D. Angosto-Bazarra, H. Martínez-Banaclocha et al., "MCC950 closes the active conformation of NLRP3 to an inactive state," *Nature Chemical Biology*, vol. 15, no. 6, pp. 560–564, 2019.

[47] Y. Li, W. Zhou, L. Yang, and R. You, "Physiological and pathological regulation of ACE2, the SARS-CoV-2 receptor," *Pharmacological Research*, vol. 157, Article ID 104833, 2020.

[48] Y.-J. Geng, Z.-Y. Wei, H.-Y. Qian, J. Huang, R. Lodato, and R. J. Castriotta, "Pathophysiological characteristics and therapeutic approaches for pulmonary injury and cardiovascular complications of coronavirus disease 2019," *Cardiovascular Pathology*, vol. 47, Article ID 107228, 2020.

[49] B. Vellingiri, K. Jayaramayya, M. Iyer et al., "COVID-19: a promising cure for the global panic," *The Science of the Total Environment*, vol. 725, Article ID 138277, 2020.

[50] F. Li, W. Li, M. Farzan, S. C. Harrison et al., "Structure of SARS coronavirus spike receptor-binding domain complexed with receptor," *Science*, vol. 309, no. 5742, pp. 1864–1868, 2005.

[51] J. Lan, J. Ge, J. Yu et al., "Structure of the SARS-CoV-2 spike receptor-binding domain bound to the ACE2 receptor," *Nature*, vol. 581, no. 7807, pp. 215–220, 2020.

[52] J. J. Mourdad and B. I. Levy, "Interaction between RAAS inhibitors and ACE2 in the context of COVID-19," *Nature Reviews Cardiology*, vol. 17, p. 313, 2020.

[53] A. M. South, D. I. Diz, and M. C. Chappell, "COVID-19, ACE2, and the cardiovascular consequences," *American Journal of Physiology—Heart and Circulatory Physiology*, vol. 318, no. 5, pp. H1084–H1090, 2020.

[54] J. Liu, R. Cao, M. Xu et al., "Hydroxychloroquine, a less toxic derivative of chloroquine, is effective in inhibiting SARS-CoV-2 infection in vitro," *Cell Discovery*, vol. 6, no. 1, pp. 16–19, 2020.

[55] S. Hraiech, J. Bourenne, K. Kuteifan et al., "Lack of viral clearance by the combination of hydroxychloroquine and azithromycin or lopinavir and ritonavir in SARS-CoV-2-related acute respiratory distress syndrome," *Annals of Intensive Care*, vol. 10, no. 1, pp. 63–66, 2020.

[56] N. J. White, J. A. Watson, R. M. Hoglund, X. H. S. Chan, P. Y. Cheah, and J. Tarning, "COVID-19 prevention and treatment: a critical analysis of chloroquine and hydroxychloroquine clinical pharmacology," *PLoS Medicine*, vol. 17, no. 9, Article ID e1003252, 2020.

[57] S.-M. Lin, S.-C. Lin, J.-N. Hsu et al., "Structure-based stabilization of non-native protein-protein interactions of coronavirus nucleocapsid proteins in antiviral drug design," *Journal of Medicinal Chemistry*, vol. 63, no. 6, pp. 3131–3141, 2020.

[58] S. M. Lin, S. C. Lin, J. N. Hsu et al., "A sequence homology and bioinformatic approach can predict candidate targets for immune responses to SARS-CoV-2," *Cell Host & Microbe*, vol. 27, pp. 671–e2, 2020.